Article

Molecular Cell

Real-Time Tracking of Parental Histones Reveals Their Contribution to Chromatin Integrity Following DNA Damage

Graphical Abstract

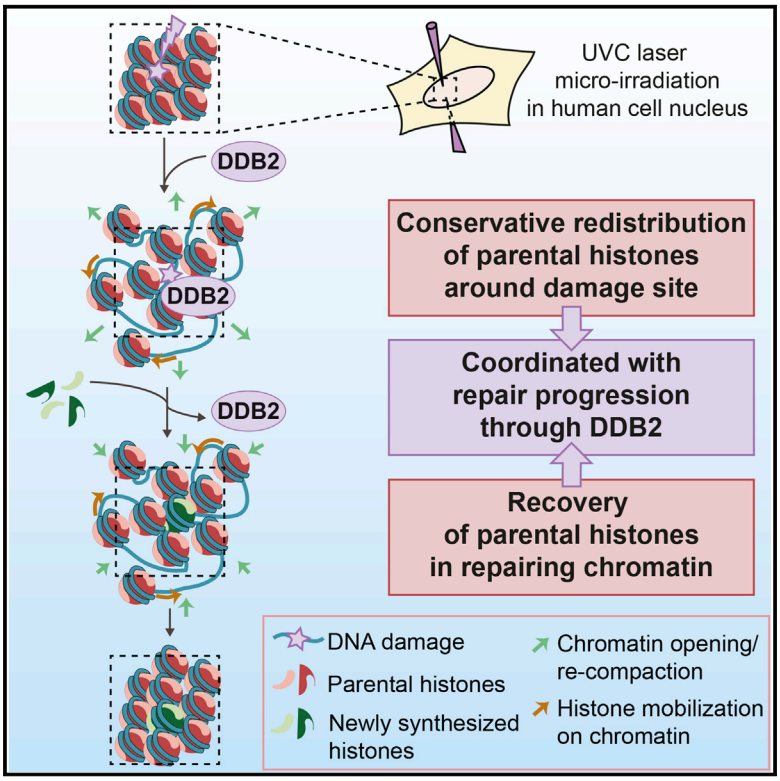

Highlights

- Parental H3 histones redistribute to the periphery of UVC-damaged regions
- The redistribution involves histone mobilization on chromatin and chromatin opening
- Parental histones recover massively during repair progression
- Parental histone dynamics may help coordinate DNA repair with epigenome integrity

Authors

Salomé Adam, Juliette Dabin, Odile Chevallier, ..., Olivier Renaud, Geneviève Almouzni, Sophie E. Polo

Correspondence

sophie.polo@univ-paris-diderot.fr

In Brief

Adam et al. identify a conservative process coordinated with UVC damage repair progression, whereby parental histones rapidly redistribute away from damaged chromatin regions and subsequently recover. Parental histone dynamics coupled to DNA repair may contribute to maintaining epigenome integrity upon DNA damage.

Adam et al., 2016, Molecular Cell *64*, 65–78
October 6, 2016
http://dx.doi.org/10.1016/j.molcel.2016.08.019

Molecular Cell
Article

Real-Time Tracking of Parental Histones Reveals Their Contribution to Chromatin Integrity Following DNA Damage

Salomé Adam,[1,2,5,6] Juliette Dabin,[1,5] Odile Chevallier,[1] Olivier Leroy,[3] Céline Baldeyron,[2,7] Armelle Corpet,[4] Patrick Lomonte,[4] Olivier Renaud,[3] Geneviève Almouzni,[2] and Sophie E. Polo[1,8,*]
[1]Epigenetics & Cell Fate Centre, UMR7216 CNRS, Paris Diderot University, Sorbonne Paris Cité, F-75013 Paris, France
[2]Laboratory of Nuclear Dynamics, UMR3664 CNRS, Institut Curie, PSL Research University, F-75005 Paris, France
[3]Plateforme Imagerie Cellulaire et Tissulaire-Infrastructure en Biologie Santé et Agronomie, UMR3215 CNRS/U934 INSERM, Institut Curie, PSL Research University, F-75005 Paris, France
[4]Team Chromatin Assembly, Nuclear Domains, Virus, Institut NeuroMyoGène, LabEx DEVweCAN, Université Claude Bernard Lyon 1, UMR5310 CNRS/U1217 INSERM, F-69100 Lyon, France
[5]Co-first author
[6]Present address: Lunenfeld-Tanenbaum Research Institute, Mount Sinai Hospital, M5G 1X5 Toronto, Canada
[7]Present address: Laboratory of Biological Dosimetry, PRP-HOM/SRBE/LDB, Institut de Radioprotection et de Sûreté Nucléaire, F-92262 Fontenay-aux-Roses, France
[8]Lead Contact
*Correspondence: sophie.polo@univ-paris-diderot.fr
http://dx.doi.org/10.1016/j.molcel.2016.08.019

SUMMARY

Chromatin integrity is critical for cell function and identity but is challenged by DNA damage. To understand how chromatin architecture and the information that it conveys are preserved or altered following genotoxic stress, we established a system for real-time tracking of parental histones, which characterize the pre-damage chromatin state. Focusing on histone H3 dynamics after local UVC irradiation in human cells, we demonstrate that parental histones rapidly redistribute around damaged regions by a dual mechanism combining chromatin opening and histone mobilization on chromatin. Importantly, parental histones almost entirely recover and mix with new histones in repairing chromatin. Our data further define a close coordination of parental histone dynamics with DNA repair progression through the damage sensor DDB2 (DNA damage-binding protein 2). We speculate that this mechanism may contribute to maintaining a memory of the original chromatin landscape and may help preserve epigenome stability in response to DNA damage.

INTRODUCTION

Cellular genomes are constantly exposed to various sources of DNA damage (Ciccia and Elledge, 2010; Hanawalt, 2015; Hoeijmakers, 2009; Jackson and Bartek, 2009), threatening not only genome stability, but also the integrity of chromatin organization (Adam et al., 2015; Lukas et al., 2011; Smeenk and van Attikum, 2013). The basic unit of chromatin is the nucleosome core particle, in which DNA is wrapped around a histone protein octamer comprising an $(H3\text{-}H4)_2$ tetramer flanked by two H2A-H2B dimers (Kornberg, 1974; Oudet et al., 1975; Luger et al., 1997). Variations at the level of this repetitive unit, through histone variants and post-translational modifications (Bannister and Kouzarides, 2011; Maze et al., 2014; Talbert and Henikoff, 2010), as well as further chromatin compaction, constitute a major source of information that regulates gene expression and cell identity (Filipescu et al., 2014; Probst et al., 2009). How chromatin is reorganized in response to DNA damage and to which extent the information that it carries can be preserved is thus of fundamental importance.

Our current view of chromatin dynamics following DNA damage in human cells is based on the Access-Repair-Restore (ARR) model (Polo and Almouzni, 2015; Smerdon, 1991). This model postulates that chromatin is first disorganized in response to DNA damage, which facilitates access to repair factors, followed by restoration of chromatin structure. Yet, it is still unclear whether, when, and by which mechanisms the pre-damage chromatin state is restored (Dabin et al., 2016). Notably, chromatin restoration after damage involves the deposition of newly synthesized histones (Adam et al., 2013; Dinant et al., 2013; Luijsterburg et al., 2016; Polo et al., 2006), which could potentially replace damaged histones and leave a mark of the damage experience. Thus, assuming that nucleosome density remains at a steady state, a subset of parental histones should be evicted from chromatin during the Access step, which would limit the capacity to recover the original epigenetic information at damaged sites (Figure 1A). Consistent with this idea, recent reports provide evidence for nucleosome destabilization and histone eviction during DNA double-strand break repair (Goldstein et al., 2013; Li and Tyler, 2016; Xu et al., 2010) and in response to UVC irradiation (Lan et al., 2012; Wang et al., 2006; Zavala et al., 2014). UVC damage sites also show reduced histone density, promoted by the UV damage sensor DDB2 (DNA

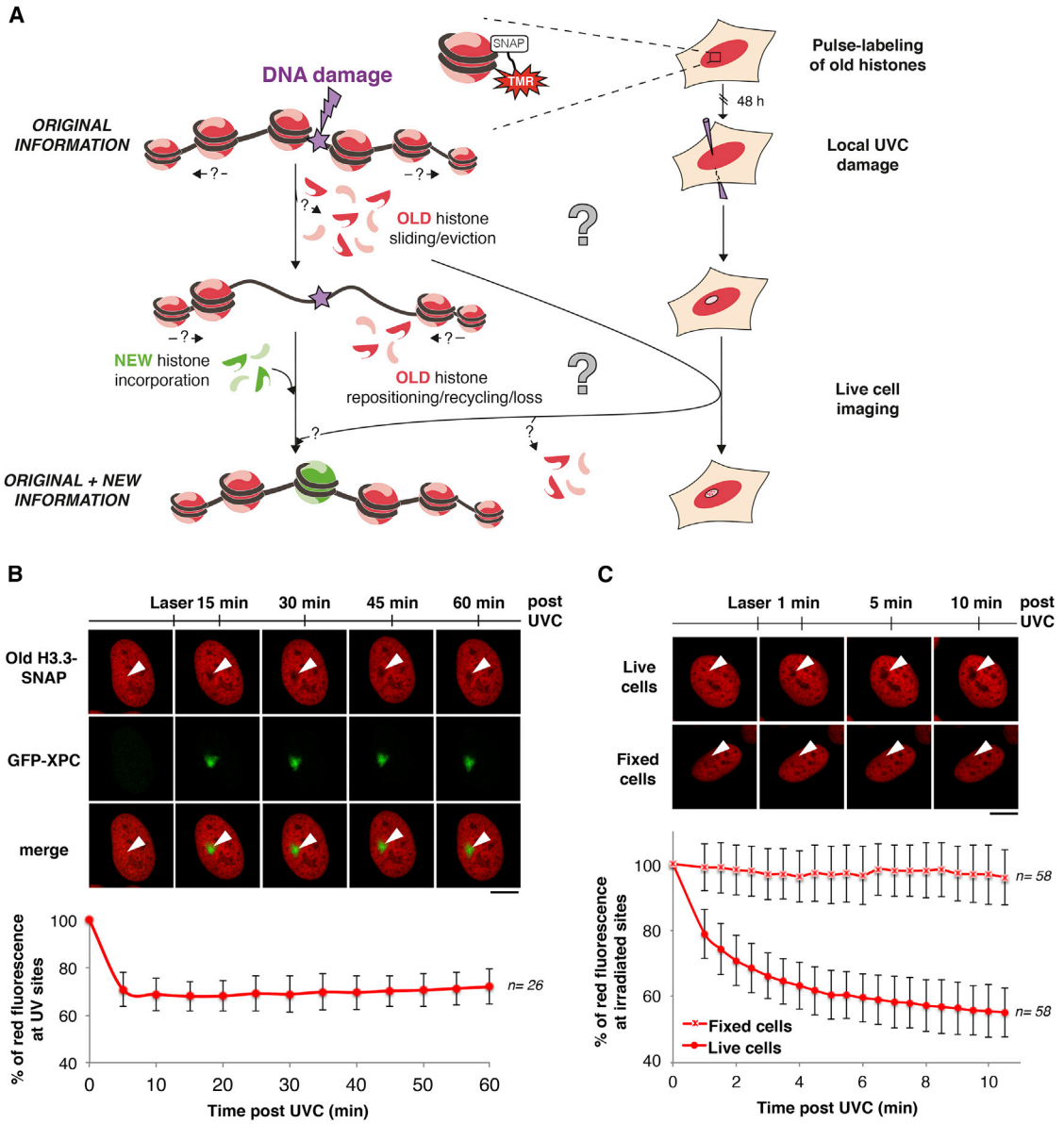

Figure 1. Rapid Decrease in Parental H3 Histone Density in UVC-Damaged Chromatin Regions

(A) Left: current model for histone dynamics in UVC-damaged chromatin (adapted from Adam et al., 2015). The incorporation of new histones (green) raises questions about the fate of parental histones (red). Right: experimental strategy for tracking parental histone dynamics at DNA damage sites.

(B) Distribution of parental histones H3.3 (red) at the indicated time points after UVC laser damage in U2OS cells stably expressing H3.3-SNAP and GFP-XPC.

(C) Dynamics of parental H3.3 (red) at early time points after local UVC damage in U2OS H3.3-SNAP cells. White arrowheads, illuminated areas. Scale bars, 10 μm. Red fluorescence measured in irradiated areas is normalized to before laser. Error bars, SD from n cells scored in two independent experiments. Labeling parental histones in green instead of red gave similar results (data not shown).

See also Figures S1 and S2 and Movie S1.

damage-binding protein 2) (Luijsterburg et al., 2012). However, a massive loss of parental histones from damaged chromatin would certainly threaten epigenome maintenance.

To fully understand how chromatin integrity is preserved or altered in response to genotoxic stress, it is critical (1) to examine the fate of parental histones present in chromatin before damage and which carry the original epigenetic information and (2) to track them long enough after damage to examine their contribution to repaired chromatin together with newly deposited histones. We developed two complementary approaches for specific tracking of parental histones following UVC damage in human cells. Challenging our current view of damaged chromatin rearrangements, we show that rather than being massively evicted and lost from damaged chromatin, parental histones redistribute in a conservative manner and subsequently recover. Our mechanistic studies demonstrate that both the redistribution

and recovery of parental histones are tightly coordinated with repair progression through the UVC damage sensor DDB2. We thus propose a conservative model by which parental histone dynamics coupled to DNA damage repair contribute to the maintenance of epigenome integrity during the response to UVC damage.

RESULTS

Rapid Reduction of Parental Histone Density in UVC-Damaged Chromatin Regions

We developed two complementary approaches combining UVC laser micro-irradiation with specific tracking of parental histones in living cells. We first took advantage of the SNAP-tag technology, which we exploited previously to follow new histone deposition at UVC damage sites (Adam et al., 2013), to fluorescently label old histones 48 hr prior to irradiation (Figure 1A). We used U2OS cells that stably express H3.3-SNAP histones (Dunleavy et al., 2011) and a GFP-tagged version of the repair factor XPC (xeroderma pigmentosum C) for visualizing damage sites in live cells (Figure S1A). Real-time imaging of parental H3.3 dynamics after local UVC irradiation revealed a rapid reduction of the red fluorescence associated with parental H3.3, which was restricted to the damaged chromatin area marked by GFP-XPC and detectable at least for 1 hr after irradiation (Figure 1B). We observed a similar decrease of parental H3.3 signal in cells that do not express GFP-XPC (Figure 1C; Movie S1), thus showing that exogenous expression of the repair factor XPC does not alter the histone response to UVC. UVC damage led to a progressive reduction of the red fluorescence associated with parental histones, with a maximum of 40% loss 10 min after DNA damage infliction (Figure 1C). We verified that the region of low histone density observed after damage did not correspond to a nucleolus (Figure S1B). We also ruled out the possibility that the decrease in parental H3.3 signal could result from photo-bleaching of the red fluorescence by the UVC laser, as irradiating paraformaldehyde-fixed cells with UVC did not reduce the red signal intensity (Figure 1C). Thus, the observed decrease in old H3.3 signal in UVC-irradiated chromatin regions actually reflects enhanced dynamics of parental H3.3 histones in response to genotoxic stress.

Considering that SNAP-tag-based labeling may interfere with parental H3 dynamics, we also developed a complementary method to track parental histones based on photo-activation of PA-GFP (photoactivatable GFP) in U2OS cells engineered to stably express H3.3-PA-GFP and RFP-XPC (Figures S1A and S1C). Consistent with our previous findings, we observed a marked reduction of parental H3.3 signal in UVC-damaged chromatin regions within minutes after laser micro-irradiation in live cells and not in paraformaldehyde-fixed cells (Figures S1D and S1E). Thus, using two distinct methods to monitor old histone dynamics, our data reveal a local loss of parental H3.3 histone signal in damaged chromatin regions. Furthermore, we observed an altered distribution of parental histones upon UVC damage in all irradiated cells throughout interphase (Figure S2A), and this was not restricted to the H3.3 variant since parental H3.1 signal was also reduced at UVC damage sites (Figures S2A and S2B). We recapitulated these results in MCF7 cancer cells and in BJ primary fibroblasts and observed similar dynamics for parental histone H4 (Figures S2C–S2F).

Collectively, these results reveal a rapid reduction of parental H3 and H4 histone density in UVC-damaged chromatin.

Conservative Redistribution of Parental Histones to the Periphery of UVC-Damaged Regions

We next sought to determine whether the local reduction in parental H3 staining upon UVC irradiation actually reflects parental histone loss from damaged chromatin. For this, we measured changes in old H3.3 fluorescence within the entire cell nucleus after local UVC damage. To maximize sensitivity in this assay, we reduced the size of the area of interest by photo-bleaching H3.3-SNAP-associated fluorescence in the whole nucleus apart from a small patch (Figure 2A). Next, photo-bleaching 40% of the fluorescence inside this patch led to a 20% fluorescence reduction in the entire nucleus (Figure 2B). In contrast, targeting UVC irradiation to the fluorescent patch, while leading to a comparable 40% loss of signal in the irradiated area, did not result in a detectable loss of fluorescence from the entire nucleus (Figure 2B). From these results, we conclude that parental H3 histones mobilized early after genotoxic stress remain in the damaged nucleus and do not undergo massive degradation, as also supported by biochemical analyses of parental H3.3 levels after UVC damage (Figure S2G).

We then refined our analysis by measuring the spatial distribution of parental H3.3 histones around the damaged area (Figure 2C). Notably, we observed that the reduction of parental histone signal in the damaged region was counterbalanced by an increase of signal in the surrounding area (Figures 2D and 2E). Importantly, this conservative redistribution of parental histones did not occur upon local photo-bleaching of parental H3.3 fluorescence (Figures 2C and 2D), and we obtained similar results by photo-activation-based tracking of parental histones (Figures S3A–S3D). Furthermore, the area showing reduced histone density gradually increased over time post-irradiation (Figure 3A), which reveals that parental histone dynamics proceed radially outward. Such redistribution of parental histones argues against their eviction from damaged chromatin, because, if solubilized in the nucleoplasm, they would not be retained in a defined space in the periphery of the irradiated region. Supporting the fact that mobilized histones remain chromatin associated, detergent extraction of live cells after UVC irradiation did not alter the redistribution pattern of parental histones (Figure S3E). Altogether, these data demonstrate that parental H3 histones redistribute to the periphery of damaged chromatin. Such redistribution can involve parental nucleosomes sliding away from DNA lesions and/or an expansion of chromatin in the irradiated region, pushing away surrounding undamaged chromatin fibers.

To test these hypotheses and gain further insights into the mechanisms underlying parental histone dynamics in UVC-damaged regions, we monitored, in parallel, histone and DNA densities. Thus, we found that parental H3.3 redistribution was accompanied by a decrease in DNA density within UVC-damaged regions (Figures 3B and S3F), indicative of chromatin opening. The area of UVC-damaged DNA increased by a factor of 1.26 within 15 min post-damage (Figure 3C), consistent with the 20% DNA density loss measured in the same experimental

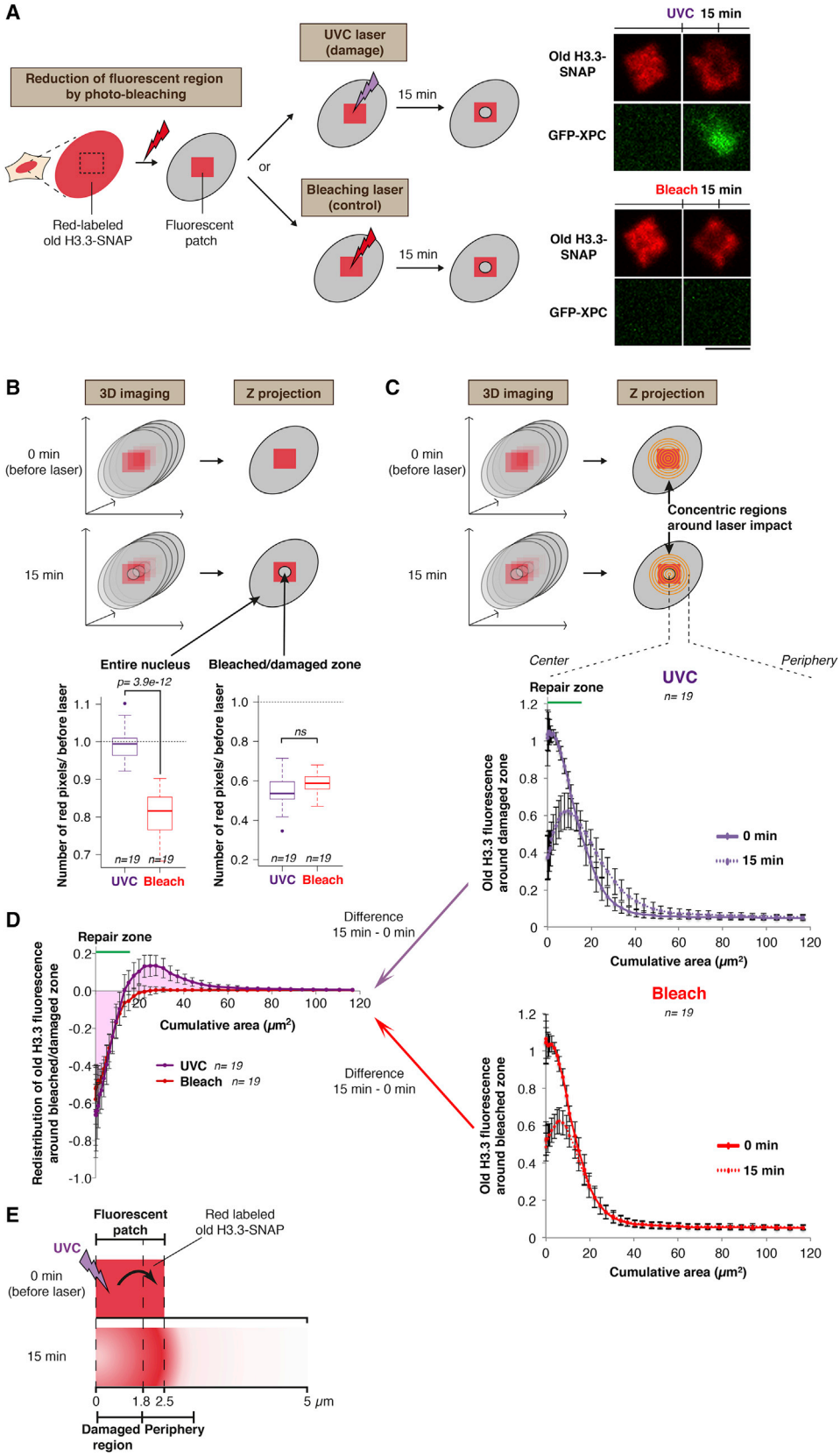

(legend on next page)

conditions (Figure 3B). This strongly supports the idea that the reduced DNA density in the damaged region results from chromatin opening. Interestingly, while histone and DNA signal loss both increased with the exposure time to UVC laser, histone signal loss exceeded DNA signal loss in all conditions examined (Figure 3D). This observation cannot be accounted for by chromatin opening only, which would lead to an equal reduction in histone and DNA densities in the damaged area. Since we already ruled out the possibility of histone dissociation from chromatin and extensive histone degradation (Figures 2 and S3), a possible explanation is that the extra loss in histone density reflects histone mobilization on chromatin away from damage sites (Figure 3E). The biphasic shape of the curves for histone and DNA signal loss as a function of UVC damage (Figure 3D) also points to a possible dual mechanism driving parental histone redistribution, each plateau corresponding to the saturation of a distinct process (Figure 3F). Our findings suggest that chromatin opening along with histone mobilization on damaged chromatin drive parental histone redistribution to the periphery of UVC-damaged regions.

The UVC Damage Sensor DDB2 Is Critical for Parental Histone Redistribution

To search for molecular determinants of parental H3 redistribution upon UVC damage, we examined the connection with UVC damage repair by knocking down factors involved at different steps in the NER (nucleotide excision repair) pathway (Figure 4A and S4A; reviewed in Alekseev and Coin, 2015; Marteijn et al., 2014). Decreasing the expression of the late repair factor XPG (xeroderma pigmentosum G), required for excision of the damaged oligonucleotide before repair synthesis, only moderately reduced parental H3.3 redistribution upon UVC irradiation (Figure S4B). Similarly, knocking down the early repair factor ERCC6 (excision repair cross-complementing 6) involved in damage recognition within transcribed genes did not markedly impair parental H3.3 dynamics (Figure S4B). Consistent with this, cells treated with a transcription inhibitor prior to UVC irradiation did not show major defects in old H3.3 redistribution (data not shown). These results indicate a relatively minor contribution of transcription-coupled repair and late repair steps to the reduced parental H3 histone density at damaged sites.

In contrast, when knocking down the UVC damage sensor DDB2 involved in global genome repair, we observed a striking impairment in parental H3.3, H3.1, and H4 density loss at UVC damage sites (Figures 4A and S4C–S4E). We did not observe comparable defects in parental H3.3 dynamics upon downregulation of XPC, another early repair factor involved in global genome repair (Figure S3F), or upon knockdown of the DDB2 partners DDB1 and CUL4A (Cullin 4A) (Figure 4A), which are part of an E3-ubiquitin ligase complex that modifies various substrates at sites of UVC damage (Nouspikel, 2011). Consistent with a minor contribution of DDB1 and CUL4A to parental H3.3 density loss, we found that preventing de novo ubiquitylation reactions by treating cells with a proteasome inhibitor or with a neddylation inhibitor did not markedly alter the redistribution of old H3.3 in damaged chromatin (Figures S4F and S4G). These data indicate that the ubiquitylation activity of the DDB1-DDB2-CUL4A-containing complex does not play a major role in parental histone dynamics following UVC damage. Parental histone redistribution to the periphery of damaged chromatin regions is thus coupled to the earliest steps of global genome NER with a prominent role for DDB2.

To further characterize the contribution of DDB2 to parental histone redistribution upon UVC damage, we tested the effect of DDB2 overexpression. Expressing exogenous DDB2 significantly increased the area of parental histone signal loss after local UVC irradiation: this area was 50% larger in cells overexpressing DDB2 than in cells overexpressing another early NER factor, XPC (Figure 4B). These results thus indicate that DDB2 levels are limiting for parental histone redistribution in UVC-irradiated chromatin regions. Furthermore, artificial tethering of DDB2 to a LacO (lactose operator) array in the absence of DNA damage led to a marked reduction of parental H3.3 histone density at the LacO array (Figure 4C). DDB2 tethering also triggered an expansion of the LacO array, as previously reported (Luijsterburg et al., 2012). These results reveal that DDB2 binding to chromatin is sufficient for parental histone redistribution even in the absence of DNA damage.

To gain mechanistic insights into DDB2 effect on parental histone dynamics, we tested the potential contribution of chromatin remodelers with reported connections to the DDB2 complex, namely ALC1 (amplified in liver cancer 1) and INO80 (inositol-requiring 80) (Jiang et al., 2010; Pines et al., 2012). Knocking down these remodelers did not recapitulate the effect of DDB2 downregulation (Figures S5A and S5B). Similarly, interfering with poly(ADP-ribosyl)ation, which has been associated with DDB2 and UV-damaged chromatin decompaction (Luijsterburg et al., 2012; Pines et al., 2012), did not impact parental histone redistribution at UVC damage sites (Figures S5C and S5D). However, our analyses of DNA and histone signal loss at UVC sites upon

Figure 2. Conservative Redistribution of Parental Histones to the Periphery of UVC-Damaged Regions

(A) Experimental procedure for measuring parental histone loss and redistribution around the UVC-damaged zone. Microscopy images show fluorescent patches of parental H3.3 (red) before and 15 min after local UVC damage (top) or photo-bleaching (bottom) in U2OS cells stably expressing H3.3-SNAP and GFP-XPC. Scale bar, 5 μm.

(B) Parental H3.3 fluorescence measured in the entire nucleus and in the bleached (red) or damaged zone (purple) 15 min post-laser micro-irradiation is normalized to before laser (dotted line). n, number of cells.

(C) Parental H3.3 fluorescence measured in concentric regions around the UVC (top graph) or bleaching laser impact (bottom graph) at the indicated time points is normalized to the fluorescence in the patch before laser.

(D) Difference in red fluorescence distribution obtained by subtracting 0 min from 15 min values quantified in (C). The positive and negative areas under the UVC curve (purple) are equivalent. The position of the repair zone is based on GFP-XPC accumulation at 15 min. Error bars, SD from n cells scored in two independent experiments.

(E) Interpretation of the results shown in (D): redistribution of old H3.3 histones to the periphery of UVC-damaged regions. Areas were converted to distances. See also Figures S2 and S3.

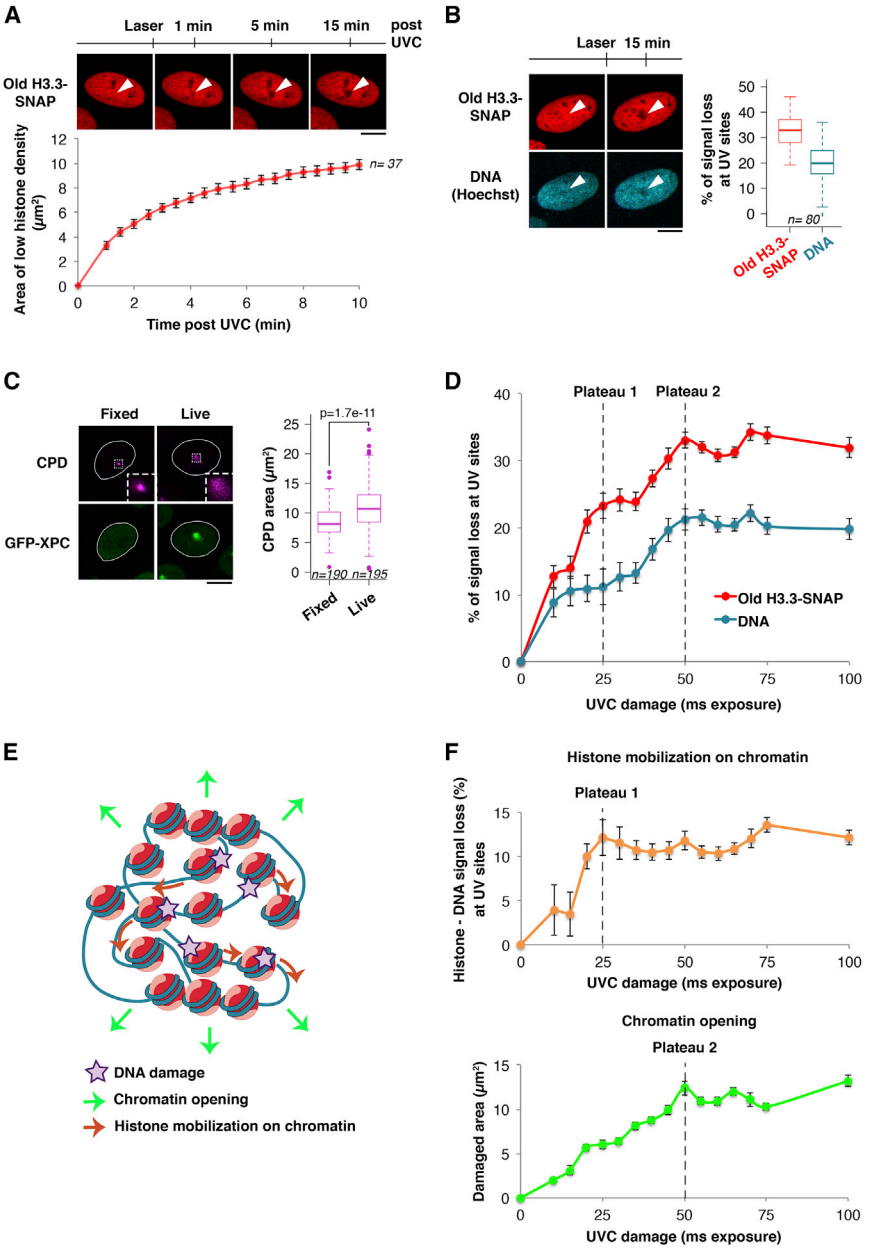

Figure 3. Chromatin Expansion and Histone Mobilization on Chromatin Contribute to Parental H3.3 Redistribution after UVC Damage

(A) Distribution of parental H3.3 (red) at the indicated time points after UVC laser damage in U2OS H3.3-SNAP cells. The area of parental histone loss is measured as a function of time post-UVC. Error bars, SEM from n cells scored in two independent experiments.

(B) Distribution of parental H3.3 (red) and DNA (blue, stained with Hoechst) before and 15 min after local UVC damage in U2OS H3.3-SNAP cells. The reduced Hoechst staining observed at damage sites is not due to photo-bleaching by the UVC laser (data not shown) or to DNA denaturation during UVC damage repair (Figure S3F). White arrowheads, irradiated areas. The boxplot shows quantifications of histone (red) and DNA (blue) fluorescence loss in irradiated areas (n cells scored in two independent experiments). Staining parental H3.3 in green and DNA in red with NUCLEAR-ID Red DNA stain gave similar results (data not shown).

(C) UVC-damaged chromatin areas visualized by staining for cyclobutane pyrimidine dimers (CPD, purple) after UVC laser damage in U2OS cells stably expressing H3.3-SNAP and GFP-XPC. The initial damaged chromatin area was measured in para-formaldehyde-fixed cells (no expansion, no GFP-XPC recruitment) and compared to 15 min after irradiation in live cells (n cells scored in two independent experiments). Insets: zoomed-in views (×3) of dashed line boxes. Scale bars, 10 μm.

(D) Quantification of parental H3.3 (red) and DNA (blue) fluorescence loss in irradiated areas as a function of UVC damage. The saturations of the two mechanisms contributing to parental histone loss (dotted lines) are obtained from the graphs in (F).

(E) Working model for parental H3.3 redistribution around UVC damage sites.

(F) Top: difference between parental H3.3 and DNA signal loss in irradiated areas as a function of UVC damage, which reflects histone mobilization on chromatin. Bottom: expansion of the damaged area marked by GFP-XPC as a function of UVC damage, indicative of chromatin opening. Dotted lines indicate the saturation of each mechanism. Error bars, SEM from at least 35 cells scored in three independent experiments.

See also Figures S3 and S5.

DDB2 knockdown (Figure S5E) indicate a major contribution of DDB2 to chromatin opening only, consistent with previous observations (Luijsterburg et al., 2012), suggesting that additional factors come into play to promote histone mobilization on chromatin.

Collectively, our data put forward the early repair factor DDB2 as a master regulator of parental histone redistribution by chromatin opening at UVC sites.

Parental H3.3 Redistribution Is Independent of New H3.3 Deposition

As we previously demonstrated that DDB2 controls the recruitment of the histone chaperone HIRA (histone regulator A), which promotes the deposition of newly synthesized histones H3.3 at UVC damage sites (Adam et al., 2013), we investigated the potential coupling between parental and new H3.3 dynamics in response to UVC irradiation. For this, we labeled parental and new histones in different colors within the same sample and compared the kinetics of parental histone density loss and new histone deposition upon local UVC damage (Figure 5A; Movies S2 and S3). While parental H3.3 histones are redistributed within minutes after damage induction, new histone H3.3 accumulation at damage sites becomes detectable only 30 min after local UVC irradiation (Figure 5A). We obtained similar results when we swapped the SNAP reagents, labeling old H3.3 in green and

new H3.3 in red (data not shown). Thus, our assay reveals that parental histone density loss precedes new histone deposition at UVC damage sites.

Given that the histone chaperone HIRA promotes the deposition of newly synthesized H3.3 at UVC damage sites (Adam et al., 2013), we tested whether the same chaperone was responsible for parental H3.3 dynamics in UVC-damaged regions. Interestingly, HIRA downregulation did not impair old H3.3 signal loss at UVC sites (Figure 5B), showing that this histone chaperone does not participate in any significant manner in parental H3.3 dynamics after UVC damage. These findings indicate that parental H3.3 redistribution likely occurs independently of new H3.3 deposition. Consistent with this, preventing the synthesis of new H3.3 by siRNA (small interfering RNA) (Figure 5C, green) did not interfere with parental H3.3 displacement from UVC-damaged regions (Figure 5C, red; note that this treatment did not affect parental H3.3 levels).

Altogether, these data demonstrate that parental histone H3.3 redistribution in UVC-damaged regions is functionally independent of new H3.3 deposition.

Recovery of Parental Histones Coupled to Repair Progression through DDB2 Release

Since parental histones are still detected in the periphery of UVC-damaged regions early after DNA damage, we investigated whether and to which extent they contribute to chromatin restoration after damage. For this purpose, we examined both parental and new H3.3 dynamics in parallel with repair progression in U2OS cells stably expressing H3.3-SNAP and CFP-XPC (Figure S6A). This analysis revealed that parental histones recovered in chromatin undergoing UVC damage repair, reaching almost complete recovery (90% of the initial signal) 9 hr after UVC irradiation, which mirrors the slow kinetics of UVC damage repair (Figure 6A). A similar extent of parental histone recovery at UVC damage sites was measured in U2OS cells stably expressing H3.3-PA-GFP (Figure S6B) and in MFC7 cells transiently expressing H3.3-SNAP (Figure S6C). Noteworthy, parental histone recovery was delayed compared to new histone incorporation (Figure 6A), suggesting that they involve distinct mechanisms. To gain insight into how parental histones recover, we compared their dynamics to basal histone mobility assessed by FRAP (fluorescence recovery after photobleaching). While parental histone recovery in UVC-damaged regions reached 80% within 12 hr after irradiation, it did not exceed 20% in an undamaged chromatin region of the same nucleus within the same time frame (Figure S6D), consistent with a previous report (Kimura and Cook, 2001). This demonstrates that parental H3.3 recovery in chromatin undergoing repair does not result from basal histone turnover but actually reflects the relocation of parental histones that were mobilized away from UVC-damaged regions. Notably, when measuring the area of parental histone density loss over time after UVC damage, we observed that parental histone recovery proceeded radially inward (Figure 6B), suggesting that displaced histones were moving back by an opposing mechanism to their initial redistribution. The area of new histone accumulation by contrast did not shrink (Figure S6E), arguing that chromatin restoration does not proceed solely via re-compaction. As a result, recovered parental histones mix with newly synthesized histones in repairing chromatin (Figure S6F).

We next sought to determine whether parental H3.3 recovery in damaged chromatin was coupled to repair progression. For this, we depleted the late repair factor XPG, which interferes with repair progression with no major effect on the early redistribution of parental histones in damaged chromatin (Figure S3B). Parental H3.3 recovery, however, was markedly impaired in XPG-depleted cells (Figure 6C; Movies S4 and S5) down to a rate similar to basal histone turnover (Figures S6D and S6G). These results indicate that parental histone recovery in damaged chromatin is dependent on repair progression. Given that XPG depletion also significantly delayed DDB2 release from chromatin, we assessed more directly the role of DDB2 in parental histone recovery. For this, we triggered LacR-DDB2 release from the LacO array by IPTG addition (Figure 6D). This resulted in rapid recovery of old H3.3 at the LacO array, which highlights the key role of DDB2 in controlling parental histone dynamics in UVC-damaged chromatin.

Collectively, our results underline the major contribution of parental histones to chromatin restoration coupled to repair and establish that parental histone recovery is coordinated with repair progression through DDB2 release from damaged chromatin.

DISCUSSION

By exploiting real-time tracking of parental H3 and H4 histones after local UVC damage in human cells, we provide novel insights into epigenome maintenance in response to DNA damage. Our study indeed identifies a conservative process, tightly coordinated with repair progression, whereby parental histones rapidly redistribute away from UVC-damaged chromatin regions and subsequently recover (Figure 7). We propose that parental histones are kept in the periphery of the damaged areas to help restore chromatin organization after DNA repair, which may contribute to preserving a memory of chromatin identity in response to DNA damage.

Parental Histone Redistribution Away from Damaged Chromatin Regions

Chromatin rearrangements coupled to the early stages of the DDR, although considered to be critical for efficient DNA repair, still remained poorly characterized. Here, we provide evidence for a redistribution of parental histones to the periphery of UVC-damaged chromatin regions, which prompt us to re-evaluate our views on the Access-Repair-Restore model. Even though histone solubilization has been reported in response to genotoxic stress (Goldstein et al., 2013; Wang et al., 2006; Xu et al., 2010), our data support a model where parental H3 histones do not massively dissociate from chromatin but are redistributed away from UVC-damaged sites, possibly via nucleosome sliding and chromatin opening. This is consistent with a recent study suggesting that H2B histones are not solubilized following UV irradiation in human cells (Morisaki and McNally, 2014).

The extent of chromatin rearrangements in response to local DNA damage is a matter of debate. While one study indicates

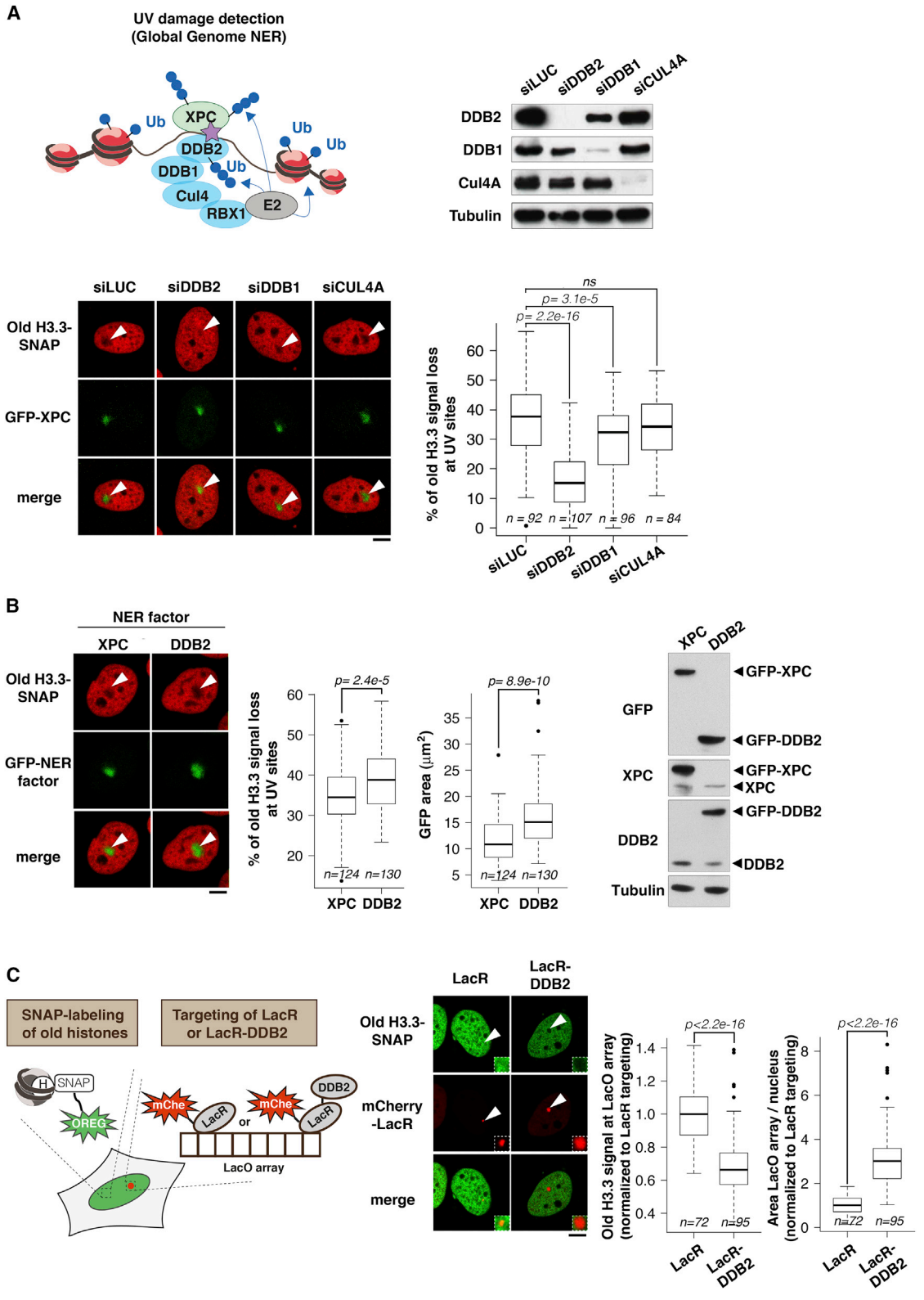

Figure 4. Parental Histone Redistribution Is Controlled by the Repair Factor DDB2

(A) Scheme representing the main repair factors involved in UVC damage detection in the global genome NER pathway. Microscopy images show the distribution of parental H3.3 (red) 15 min after UVC laser damage in U2OS cells stably expressing H3.3-SNAP and GFP-XPC treated with the indicated siRNAs

(legend continued on next page)

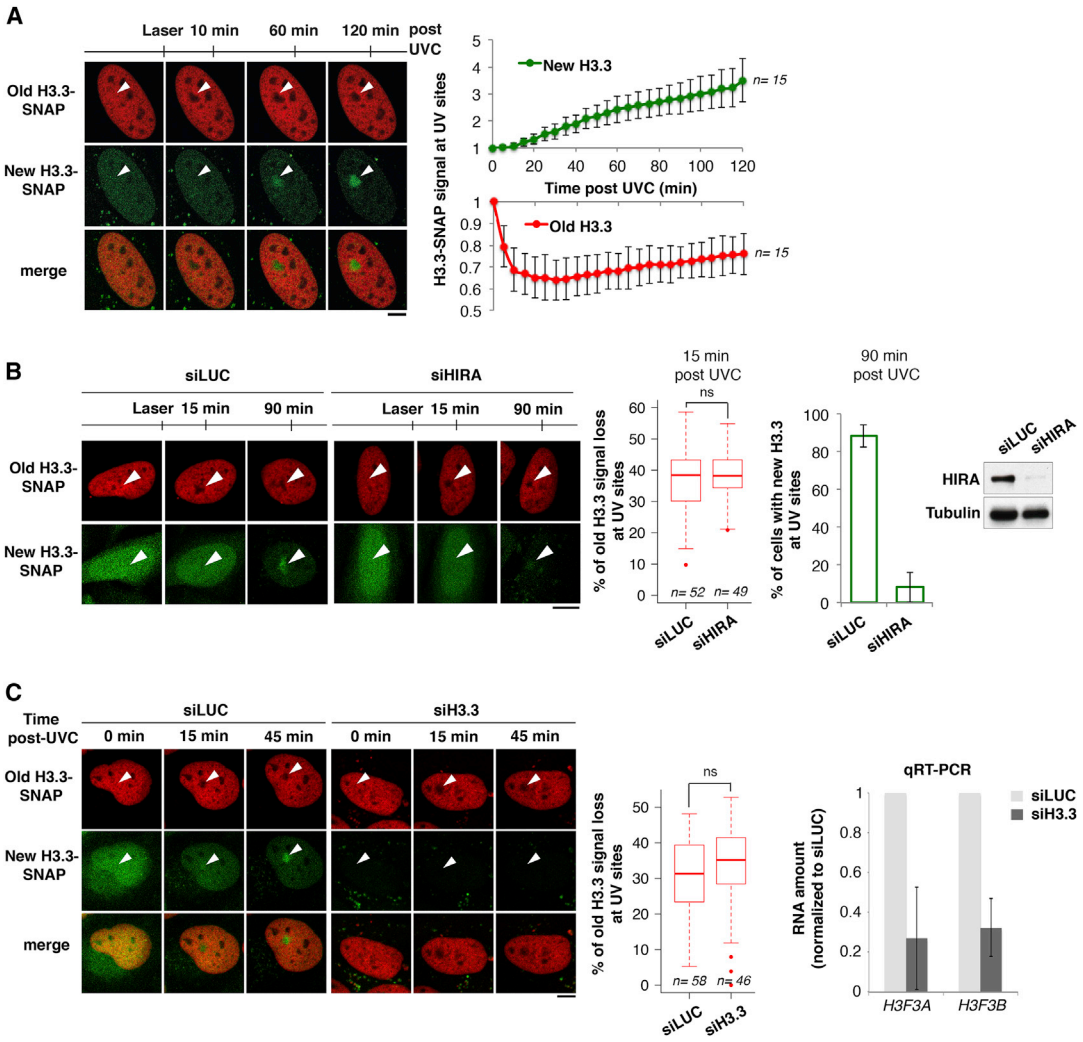

Figure 5. Parental H3.3 Redistribution Is Independent of New H3.3 Deposition

(A) Dynamics of parental (red) and new H3.3 (green) at the indicated time points after UVC laser damage in U2OS H3.3-SNAP cells. Red and green signals measured in damaged areas are normalized to before laser. Error bars, SD from n cells scored in two independent experiments.

(B) Distribution of parental and new H3.3 as in (A) in cells treated with the indicated siRNAs (siLUC: control). HIRA knockdown is verified by western blot and by the inhibition of new H3.3 deposition at damage sites.

(C) Distribution of parental and new H3.3 as in (B). siRNA efficiency was verified by qRT-PCR. Error bars, SD from two independent experiments. Red fluorescence loss is measured in damaged areas at 15 min compared to before laser (n cells scored in two independent experiments). White arrowheads, irradiated areas. Scale bars, 10 μm.

See also Movies S2 and S3.

that chromatin destabilization affects the whole nucleus upon local UVC irradiation (Rubbi and Milner, 2003), several lines of evidence rather support the idea that chromatin is locally disorganized upon genotoxic stress (Dinant et al., 2013; Goldstein et al., 2013; Hinde et al., 2014; Kruhlak et al., 2006; Luijsterburg et al., 2012; Smeenk et al., 2013). Here, we reconcile these data

(siLUC: control). siRNA efficiencies were verified by western blot. The red fluorescence loss measured in damaged areas is normalized to before laser (n cells scored in two independent experiments).

(B) Distribution of parental H3.3 (red) 15 min after UVC laser damage in U2OS cells stably expressing H3.3-SNAP and GFP-XPC or GFP-DDB2. Expression levels of exogenous XPC and DDB2 relative to the endogenous proteins are shown on the western blot. Red fluorescence loss is measured in irradiated areas relative to before laser and the area of fluorescence loss is marked by GFP-tagged NER factors.

(C) Distribution of parental H3.3 (green) upon tethering of mCherry-LacR (LacR) or mCherry-LacR-DDB2 (LacR-DDB2) to the LacO array in U2OS LacO cells stably expressing H3.3-SNAP. The area of the LacO array and green fluorescence at the LacO array are displayed on the boxplots (n cells scored in two independent experiments). White arrowheads, irradiated areas or LacO array. Scale bars, 10 μm.

See also Figures S4 and S5.

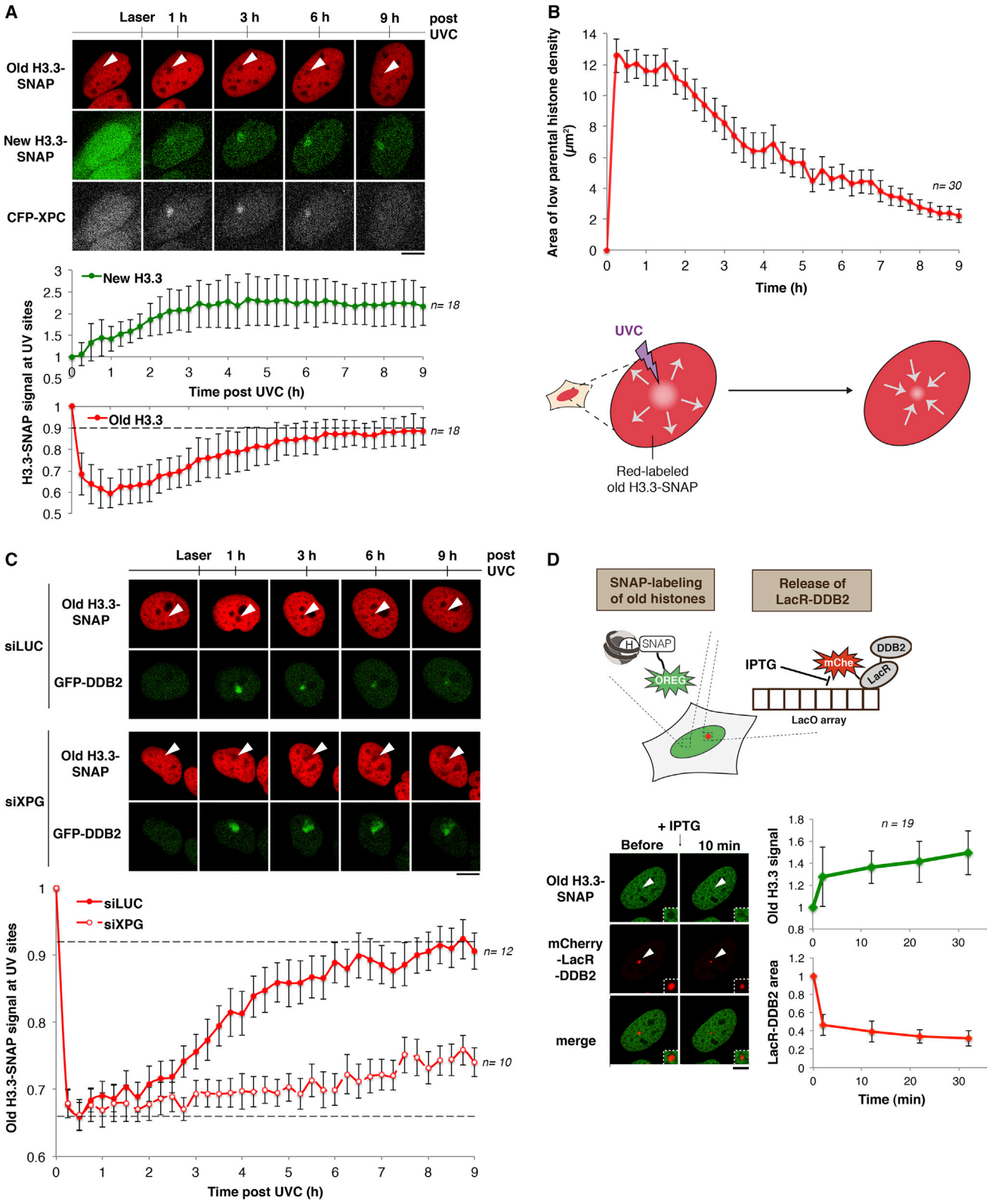

(legend on next page)

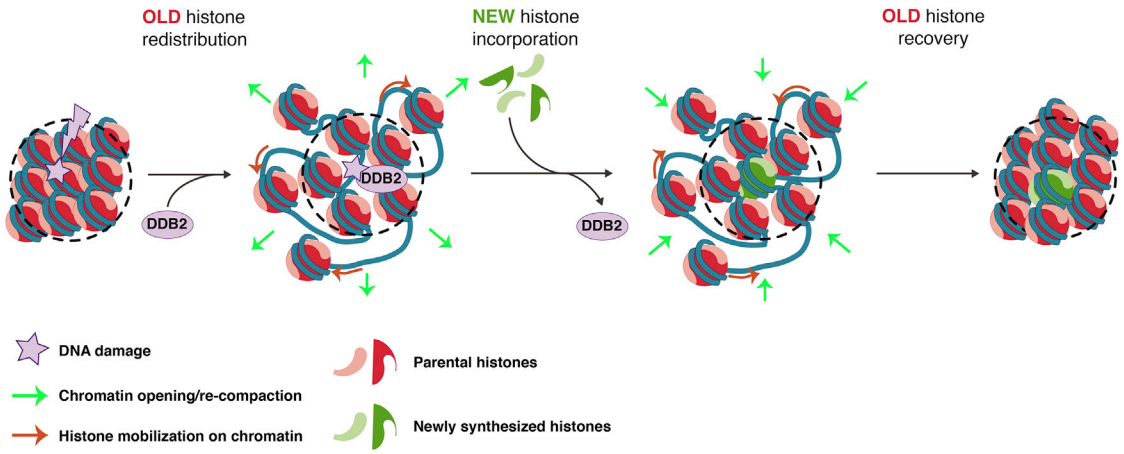

Figure 7. Model for Parental Histone Dynamics Coupled to Repair in UVC-Damaged Chromatin

UVC damage leads to the redistribution of parental histones to the periphery of damaged chromatin regions. This occurs via a decompaction of damaged chromatin, which pushes away the surrounding undamaged chromatin fibers, along with a mobilization of parental histones on chromatin away from damage sites, making room for new histone incorporation. Restoration of the overall chromatin organization proceeds by chromatin re-compaction and sliding back the nucleosomes bearing parental histones. The whole process is tightly coordinated with DNA repair progression through binding and release of the damage sensor DDB2.

by demonstrating that a local loss of parental histone density in UVC-damaged areas has a long-range impact on chromatin, potentially affecting the whole nucleus, because parental histone redistribution actually spreads over long distances away from the damaged regions (Figure 2E).

Whether and how histone redistribution facilitates access to damaged DNA and repair progression are not entirely clear. The recruitment of the damage sensor DDB2 to UVC lesions precedes and orchestrates parental histone dynamics. Mobilizing parental histones may be necessary for recruiting downstream NER factors to damaged chromatin. It is tempting to speculate that this may also contribute to protect parental histones from modifications by histone-modifying enzymes recruited to regions of ongoing repair, thereby promoting the maintenance of the original epigenetic information.

Mechanistically, both histone mobilization on chromatin and chromatin opening potentially contribute to chromatin disorganization in response to UVC damage. Whether they use similar regulatory factors as those promoting chromatin mobility in response to DNA breaks (Dion and Gasser, 2013) is an attractive possibility. In terms of molecular players, we identify the damage sensor DDB2 as a master regulator of parental histone dynamics at sites of UVC lesions, mostly via its ability to promote chromatin opening. Interestingly, while the ubiquitylation activity of DDB2-containing complex is required for new histone deposition in UVC-damaged chromatin (Adam et al., 2013), it is largely dispensable for parental histone dynamics. Consistent with our findings, ubiquitylation-deficient mutants of DDB2 induce chromatin expansion like wild-type DDB2 when artificially tethered to chromatin (Luijsterburg et al., 2012). Thus, DDB2-mediated chromatin expansion is largely independent of the other members of the UVC damage recognition complex. Whether DDB2 acts alone or in association with other factors to fulfill this activity will be important to investigate in future studies. Remarkably, DDB2 has very strong affinity for UVC-damaged DNA (Kulaksiz et al., 2005; Wittschieben et al., 2005), and DDB2 binds damaged DNA on nucleosomes (Osakabe et al., 2015). We can speculate that DDB2 binding to damaged chromatin may on its own push away surrounding nucleofilaments leading to chromatin opening. Given that DDB2 does not display ATPase/helicase or histone-binding domains, we rather favor a model where it works in concert with other factors directly involved in

Figure 6. Recovery of Parental Histones Coupled to Repair Progression

(A) Dynamics of parental (red) and new H3.3 (green) at the indicated time points after UVC laser damage in U2OS cells stably expressing H3.3-SNAP and CFP-XPC. Green and red signals are quantified in irradiated areas relative to before laser. Cells that did not repair efficiently (based on CFP-XPC retention) were excluded from the analysis. Error bars, SD from n cells scored in two independent experiments. Staining parental histones in green and new histones in red gave similar results (not shown).

(B) Area of parental H3.3 histone loss as a function of time post-UVC irradiation, reflecting opening and closure of the damaged zone. Error bars, SEM from n cells scored in two independent experiments.

(C) Dynamics of parental H3.3 (red) at the indicated time points after UVC laser damage in U2OS cells stably expressing H3.3-SNAP and GFP-DDB2 treated with the indicated siRNAs (siLUC: control). The efficiency of XPG depletion is indicated by sustained retention of GFP-DDB2 at UV sites. Red fluorescence measured in damaged areas is normalized to before laser. Error bars, SEM from n cells scored in two independent experiments.

(D) Distribution of parental H3.3 (green) upon IPTG-mediated release of mCherry-LacR-DDB2 from the LacO array in U2OS LacO cells stably expressing H3.3-SNAP. The green fluorescence at the LacO array and LacR-DDB2 area (red) measured after IPTG addition are normalized to before IPTG. Error bars, SD from n cells scored in two independent experiments. White arrowheads, irradiated areas or LacO array. Scale bars, 10 μm.

See also Figure S6 and Movies S4 and S5.

chromatin dynamics—such as histone chaperones and/or chromatin remodeling complexes that remain to be identified—to promote chromatin disorganization in damaged regions.

Epigenome Maintenance after DNA Damage

Our study identifies a pathway that may contribute to preserving the integrity of chromatin architecture in response to DNA damage. We unraveled that damaged chromatin reorganization is a two-step process with new histone incorporation preceding parental histone recovery. The biphasic nature of chromatin restoration is consistent with an early model based on the accessibility to nucleases of chromatin undergoing NER (reviewed in Smerdon, 1991).

While we cannot formally exclude that a limited amount of parental histones are ultimately degraded after UVC damage as reported for hyperacetylated histones in response to ionizing radiation (Qian et al., 2013), the conservative nature of parental histone redistribution around UVC damage sites and the almost complete recovery of parental histones during repair progression argue against massive histone degradation. Furthermore, the retention of parental histones proximal to the site of damage offers a possible redirection to the original site to promote a conservative restoration of chromatin architecture. It will be important to develop higher-resolution approaches to determine whether parental histones retrieve their original positions on the DNA sequence upon recovery and whether the topological organization of parental chromatin is fully re-established.

The major contribution of parental histones to the composition of repaired chromatin is crucial to envision mechanisms for epigenome maintenance after DNA damage. Indeed, it opens up the possibility that parental marks can be preserved and transferred to the new histones, which initially carry their own set of post-translational modifications (PTMs) (Loyola et al., 2006). In this respect, a parallel can be drawn between the restoration of chromatin after DNA damage and DNA replication (Alabert and Groth, 2012; Groth et al., 2007; MacAlpine and Almouzni, 2013).

At the replication fork, the maintenance of chromatin identity is achieved by old histone recycling with their PTMs and by subsequent modifications of new histones to mirror the parental ones (Alabert et al., 2015). Whether similar mechanisms operate in damaged chromatin is an attractive possibility. Noteworthy, while cells have to cope with 50% histone renewal during replication, most parental histones recover in damaged chromatin regions, which could facilitate the re-establishment of the original chromatin landscape. It is tempting to speculate that the presence of parental and new histones in neighboring nucleosomes may allow old PTM transmission to newly deposited histones after repair.

Finally, our data open up new avenues for understanding the etiology of several human diseases, including H3 mutant-associated cancers (reviewed in Kallappagoudar et al., 2015; Yuen and Knoepfler, 2013) and NER disorders (reviewed in DiGiovanna and Kraemer, 2012; Marteijn et al., 2014). Considering that DDB2 dynamics strongly impact the fate of parental histones in response to UVC damage, the phenotype of XPE patients harboring DDB2 mutations that prevent its binding to damaged DNA may not only reflect a DNA repair defect but also altered chromatin plasticity in response to genotoxic stress. Similarly, H3 mutations could contribute to the development of human cancers by affecting the resetting of the epigenome following DNA damage.

In conclusion, our work sheds new light to our current view of DNA damage-induced chromatin rearrangements and suggests that parental histone dynamics are critical to the maintenance of epigenome integrity in response to genotoxic stress. Our findings also pave the way for the identification of new factors that contribute to restoring damaged chromatin identity and for understanding how this protects cells against pathological conditions.

EXPERIMENTAL PROCEDURES

Cell Culture and Drug Treatments

All cell lines and drug treatments are described in the Supplemental Experimental Procedures.

SNAP Labeling and Photo-activation of Histones

SNAP labeling of histone proteins was done as described (Bodor et al., 2012). Photo-activation experiments were performed in U2OS cells stably expressing H3.3-PA-GFP on a Zeiss LSM710 confocal microscope using the 30 mW 405 nm laser focused through an LD LCI Plan-Apochromat 25×/0.8 oil objective. See Supplemental Experimental Procedures for details.

UVC Laser Micro-irradiation and FRAP

UVC laser micro-irradiation was done as described (Adam et al., 2013; Dinant et al., 2007). Details for the FRAP procedure and for image acquisition and analysis are in Supplemental Experimental Procedures.

siRNA and Plasmid Transfections

siRNAs (Supplemental Experimental Procedures) were transfected into cells using Lipofectamine RNAiMAX (Invitrogen). Cells were transiently transfected with plasmid DNA (1 μg/mL final, Supplemental Experimental Procedures) using Lipofectamine 2000 (Invitrogen) 48 hr before subsequent cell treatment.

Cell Extracts and Western Blot, Immunofluorescence, and qRT-PCR

These procedures, including lists of antibodies and primer pairs, are described in Supplemental Experimental Procedures.

Statistical Analysis

p values for mean comparisons between two groups were calculated with a Student's t test, including Welch's correction when necessary, using R software. Multiple comparisons were performed by one-way ANOVA with Bonferroni post-test using GraphPad Prism.

SUPPLEMENTAL INFORMATION

Supplemental Information includes Supplemental Experimental Procedures, six figures, and five movies and can be found with this article online at http://dx.doi.org/10.1016/j.molcel.2016.08.019.

AUTHOR CONTRIBUTIONS

S.A., J.D. (equal contribution), and S.E.P. designed and performed experiments, analyzed the data, and wrote the manuscript. O.C. provided technical assistance. C.B. designed the UVC laser microscope set-up for G.A.'s lab. O.L. and O.R. implemented the UVC laser technology and helped with image analyses. A.C. produced the BJ H3.1-SNAP cell line in P.L.'s lab. S.E.P. and G.A. co-directed S.A.'s work. G.A. provided inputs for experimental design using the UVC laser technology and SNAP tagging and for data analysis and writing. S.E.P. supervised the project.

ACKNOWLEDGMENTS

We thank our colleagues for fruitful discussions and critical reading of the manuscript. N. Dantuma, E. Dunleavy, S. Jackson, L. Jansen, J. Lippincott-Schwartz, R. Nishi, and H. van Attikum shared reagents. The ImagoSeine core facility (Institut Jacques Monod, France BioImaging) assisted with confocal microscopy. This work was supported by the European Research Council (ERC-2013-StG-336427 "EpIn"), the French National Research Agency (ANR-12-JSV6-0002-01, "Who am I"? LabEx ANR-11-LABX-0071, ANR-11-IDEX-0005-01, France-BioImaging ANR-10-INSB-04), EDF Radiobiology program RB 2014-01, and the Fondation ARC. Research in G.A. group is supported by la Ligue Nationale contre le Cancer (Equipe labellisée), the European Commission Network of Excellence EpiGeneSys (HEALTH-F4-2010-257082), ERC-2009-AdG_20090506 "Eccentric," ANR-11-LABX-0044_DEEP, and ANR-10-IDEX-0001-02 PSL*. P.L.'s group is funded by VIRUCEPTION (ANR-13-BSV3-0001-01) and the LabEx DEVweCAN (ANR-10-LABX-61). S.A. received PhD fellowships from University Pierre et Marie Curie and La Ligue contre le Cancer. J.D. received a PhD fellowship from University Paris Diderot.

Received: March 21, 2016
Revised: June 20, 2016
Accepted: August 11, 2016
Published: September 15, 2016

REFERENCES

Adam, S., Polo, S.E., and Almouzni, G. (2013). Transcription recovery after DNA damage requires chromatin priming by the H3.3 histone chaperone HIRA. Cell *155*, 94–106.

Adam, S., Dabin, J., and Polo, S.E. (2015). Chromatin plasticity in response to DNA damage: the shape of things to come. DNA Repair (Amst.) *32*, 120–126.

Alabert, C., and Groth, A. (2012). Chromatin replication and epigenome maintenance. Nat. Rev. Mol. Cell Biol. *13*, 153–167.

Alabert, C., Barth, T.K., Reverón-Gómez, N., Sidoli, S., Schmidt, A., Jensen, O.N., Imhof, A., and Groth, A. (2015). Two distinct modes for propagation of histone PTMs across the cell cycle. Genes Dev. *29*, 585–590.

Alekseev, S., and Coin, F. (2015). Orchestral maneuvers at the damaged sites in nucleotide excision repair. Cell. Mol. Life Sci. *72*, 2177–2186.

Bannister, A.J., and Kouzarides, T. (2011). Regulation of chromatin by histone modifications. Cell Res. *21*, 381–395.

Bodor, D.L., Rodríguez, M.G., Moreno, N., and Jansen, L.E.T. (2012). Analysis of protein turnover by quantitative SNAP-based pulse-chase imaging. Curr. Protoc. Cell Biol. *Chapter 8*, Unit8.8.

Ciccia, A., and Elledge, S.J. (2010). The DNA damage response: making it safe to play with knives. Mol. Cell *40*, 179–204.

Dabin, J., Fortuny, A., and Polo, S.E. (2016). Epigenome maintenance in response to DNA damage. Mol. Cell *62*, 712–727.

DiGiovanna, J.J., and Kraemer, K.H. (2012). Shining a light on xeroderma pigmentosum. J. Invest. Dermatol. *132*, 785–796.

Dinant, C., de Jager, M., Essers, J., van Cappellen, W.A., Kanaar, R., Houtsmuller, A.B., and Vermeulen, W. (2007). Activation of multiple DNA repair pathways by sub-nuclear damage induction methods. J. Cell Sci. *120*, 2731–2740.

Dinant, C., Ampatziadis-Michailidis, G., Lans, H., Tresini, M., Lagarou, A., Grosbart, M., Theil, A.F., van Cappellen, W.A., Kimura, H., Bartek, J., et al. (2013). Enhanced chromatin dynamics by FACT promotes transcriptional restart after UV-induced DNA damage. Mol. Cell *51*, 469–479.

Dion, V., and Gasser, S.M. (2013). Chromatin movement in the maintenance of genome stability. Cell *152*, 1355–1364.

Dunleavy, E.M., Almouzni, G., and Karpen, G.H. (2011). H3.3 is deposited at centromeres in S phase as a placeholder for newly assembled CENP-A in G_1 phase. Nucleus *2*, 146–157.

Filipescu, D., Müller, S., and Almouzni, G. (2014). Histone H3 variants and their chaperones during development and disease: contributing to epigenetic control. Annu. Rev. Cell Dev. Biol. *30*, 615–646.

Goldstein, M., Derheimer, F.A., Tait-Mulder, J., and Kastan, M.B. (2013). Nucleolin mediates nucleosome disruption critical for DNA double-strand break repair. Proc. Natl. Acad. Sci. USA *110*, 16874–16879.

Groth, A., Rocha, W., Verreault, A., and Almouzni, G. (2007). Chromatin challenges during DNA replication and repair. Cell *128*, 721–733.

Hanawalt, P.C. (2015). Historical perspective on the DNA damage response. DNA Repair (Amst.) *36*, 2–7.

Hinde, E., Kong, X., Yokomori, K., and Gratton, E. (2014). Chromatin dynamics during DNA repair revealed by pair correlation analysis of molecular flow in the nucleus. Biophys. J. *107*, 55–65.

Hoeijmakers, J.H.J. (2009). DNA damage, aging, and cancer. N. Engl. J. Med. *361*, 1475–1485.

Jackson, S.P., and Bartek, J. (2009). The DNA-damage response in human biology and disease. Nature *461*, 1071–1078.

Jiang, Y., Wang, X., Bao, S., Guo, R., Johnson, D.G., Shen, X., and Li, L. (2010). INO80 chromatin remodeling complex promotes the removal of UV lesions by the nucleotide excision repair pathway. Proc. Natl. Acad. Sci. USA *107*, 17274–17279.

Kallappagoudar, S., Yadav, R.K., Lowe, B.R., and Partridge, J.F. (2015). Histone H3 mutations—a special role for H3.3 in tumorigenesis? Chromosoma *124*, 177–189.

Kimura, H., and Cook, P.R. (2001). Kinetics of core histones in living human cells: little exchange of H3 and H4 and some rapid exchange of H2B. J. Cell Biol. *153*, 1341–1353.

Kornberg, R.D. (1974). Chromatin structure: a repeating unit of histones and DNA. Science *184*, 868–871.

Kruhlak, M.J., Celeste, A., Dellaire, G., Fernandez-Capetillo, O., Müller, W.G., McNally, J.G., Bazett-Jones, D.P., and Nussenzweig, A. (2006). Changes in chromatin structure and mobility in living cells at sites of DNA double-strand breaks. J. Cell Biol. *172*, 823–834.

Kulaksiz, G., Reardon, J.T., and Sancar, A. (2005). Xeroderma pigmentosum complementation group E protein (XPE/DDB2): purification of various complexes of XPE and analyses of their damaged DNA binding and putative DNA repair properties. Mol. Cell. Biol. *25*, 9784–9792.

Lan, L., Nakajima, S., Kapetanaki, M.G., Hsieh, C.L., Fagerburg, M., Thickman, K., Rodriguez-Collazo, P., Leuba, S.H., Levine, A.S., and Rapić-Otrin, V. (2012). Monoubiquitinated histone H2A destabilizes photolesion-containing nucleosomes with concomitant release of UV-damaged DNA-binding protein E3 ligase. J. Biol. Chem. *287*, 12036–12049.

Li, X., and Tyler, J.K. (2016). Nucleosome disassembly during human non-homologous end joining followed by concerted HIRA- and CAF-1-dependent reassembly. eLife *5*, 5.

Loyola, A., Bonaldi, T., Roche, D., Imhof, A., and Almouzni, G. (2006). PTMs on H3 variants before chromatin assembly potentiate their final epigenetic state. Mol. Cell *24*, 309–316.

Luger, K., Mäder, A.W., Richmond, R.K., Sargent, D.F., and Richmond, T.J. (1997). Crystal structure of the nucleosome core particle at 2.8 A resolution. Nature *389*, 251–260.

Luijsterburg, M.S., Lindh, M., Acs, K., Vrouwe, M.G., Pines, A., van Attikum, H., Mullenders, L.H., and Dantuma, N.P. (2012). DDB2 promotes chromatin decondensation at UV-induced DNA damage. J. Cell Biol. *197*, 267–281.

Luijsterburg, M.S., de Krijger, I., Wiegant, W.W., Shah, R.G., Smeenk, G., de Groot, A.J.L., Pines, A., Vertegaal, A.C.O., Jacobs, J.J.L., Shah, G.M., and van Attikum, H. (2016). PARP1 links CHD2-mediated chromatin expansion and H3.3 deposition to DNA repair by non-homologous end joining. Mol. Cell *61*, 547–562.

Lukas, J., Lukas, C., and Bartek, J. (2011). More than just a focus: rhe chromatin response to DNA damage and its role in genome integrity maintenance. Nat. Cell Biol. *13*, 1161–1169.

MacAlpine, D.M., and Almouzni, G. (2013). Chromatin and DNA replication. Cold Spring Harb. Perspect. Biol. *5*, a010207–a010207.

Marteijn, J.A., Lans, H., Vermeulen, W., and Hoeijmakers, J.H.J. (2014). Understanding nucleotide excision repair and its roles in cancer and ageing. Nat. Rev. Mol. Cell Biol. *15*, 465–481.

Maze, I., Noh, K.-M., Soshnev, A.A., and Allis, C.D. (2014). Every amino acid matters: essential contributions of histone variants to mammalian development and disease. Nat. Rev. Genet. *15*, 259–271.

Morisaki, T., and McNally, J.G. (2014). Photoswitching-free FRAP analysis with a genetically encoded fluorescent tag. PLoS ONE *9*, e107730.

Nouspikel, T. (2011). Multiple roles of ubiquitination in the control of nucleotide excision repair. Mech. Ageing Dev. *132*, 355–365.

Osakabe, A., Tachiwana, H., Kagawa, W., Horikoshi, N., Matsumoto, S., Hasegawa, M., Matsumoto, N., Toga, T., Yamamoto, J., Hanaoka, F., et al. (2015). Structural basis of pyrimidine-pyrimidone (6-4) photoproduct recognition by UV-DDB in the nucleosome. Sci. Rep. *5*, 16330.

Oudet, P., Gross-Bellard, M., and Chambon, P. (1975). Electron microscopic and biochemical evidence that chromatin structure is a repeating unit. Cell *4*, 281–300.

Pines, A., Vrouwe, M.G., Marteijn, J.A., Typas, D., Luijsterburg, M.S., Cansoy, M., Hensbergen, P., Deelder, A., de Groot, A., Matsumoto, S., et al. (2012). PARP1 promotes nucleotide excision repair through DDB2 stabilization and recruitment of ALC1. J. Cell Biol. *199*, 235–249.

Polo, S.E., and Almouzni, G. (2015). Chromatin dynamics after DNA damage: the legacy of the access-repair-restore model. DNA Repair (Amst.) *36*, 114–121.

Polo, S.E., Roche, D., and Almouzni, G. (2006). New histone incorporation marks sites of UV repair in human cells. Cell *127*, 481–493.

Probst, A.V., Dunleavy, E., and Almouzni, G. (2009). Epigenetic inheritance during the cell cycle. Nat. Rev. Mol. Cell Biol. *10*, 192–206.

Qian, M.-X., Pang, Y., Liu, C.H., Haratake, K., Du, B.-Y., Ji, D.-Y., Wang, G.-F., Zhu, Q.-Q., Song, W., Yu, Y., et al. (2013). Acetylation-mediated proteasomal degradation of core histones during DNA repair and spermatogenesis. Cell *153*, 1012–1024.

Rubbi, C.P., and Milner, J. (2003). p53 is a chromatin accessibility factor for nucleotide excision repair of DNA damage. EMBO J. *22*, 975–986.

Smeenk, G., and van Attikum, H. (2013). The chromatin response to DNA breaks: leaving a mark on genome integrity. Annu. Rev. Biochem. *82*, 55–80.

Smeenk, G., Wiegant, W.W., Marteijn, J.A., Luijsterburg, M.S., Sroczynski, N., Costelloe, T., Romeijn, R.J., Pastink, A., Mailand, N., Vermeulen, W., and van Attikum, H. (2013). Poly(ADP-ribosyl)ation links the chromatin remodeler SMARCA5/SNF2H to RNF168-dependent DNA damage signaling. J. Cell Sci. *126*, 889–903.

Smerdon, M.J. (1991). DNA repair and the role of chromatin structure. Curr. Opin. Cell Biol. *3*, 422–428.

Talbert, P.B., and Henikoff, S. (2010). Histone variants—ancient wrap artists of the epigenome. Nat. Rev. Mol. Cell Biol. *11*, 264–275.

Wang, H., Zhai, L., Xu, J., Joo, H.-Y., Jackson, S., Erdjument-Bromage, H., Tempst, P., Xiong, Y., and Zhang, Y. (2006). Histone H3 and H4 ubiquitylation by the CUL4-DDB-ROC1 ubiquitin ligase facilitates cellular response to DNA damage. Mol. Cell *22*, 383–394.

Wittschieben, B.Ø., Iwai, S., and Wood, R.D. (2005). DDB1-DDB2 (xeroderma pigmentosum group E) protein complex recognizes a cyclobutane pyrimidine dimer, mismatches, apurinic/apyrimidinic sites, and compound lesions in DNA. J. Biol. Chem. *280*, 39982–39989.

Xu, Y., Sun, Y., Jiang, X., Ayrapetov, M.K., Moskwa, P., Yang, S., Weinstock, D.M., and Price, B.D. (2010). The p400 ATPase regulates nucleosome stability and chromatin ubiquitination during DNA repair. J. Cell Biol. *191*, 31–43.

Yuen, B.T.K., and Knoepfler, P.S. (2013). Histone H3.3 mutations: a variant path to cancer. Cancer Cell *24*, 567–574.

Zavala, A.G., Morris, R.T., Wyrick, J.J., and Smerdon, M.J. (2014). High-resolution characterization of CPD hotspot formation in human fibroblasts. Nucleic Acids Res. *42*, 893–905.

Molecular Cell, Volume *64*

Supplemental Information

Real-Time Tracking of Parental Histones Reveals Their Contribution to Chromatin Integrity Following DNA Damage

Salomé Adam, Juliette Dabin, Odile Chevallier, Olivier Leroy, Céline Baldeyron, Armelle Corpet, Patrick Lomonte, Olivier Renaud, Geneviève Almouzni, and Sophie E. Polo

Figure S1

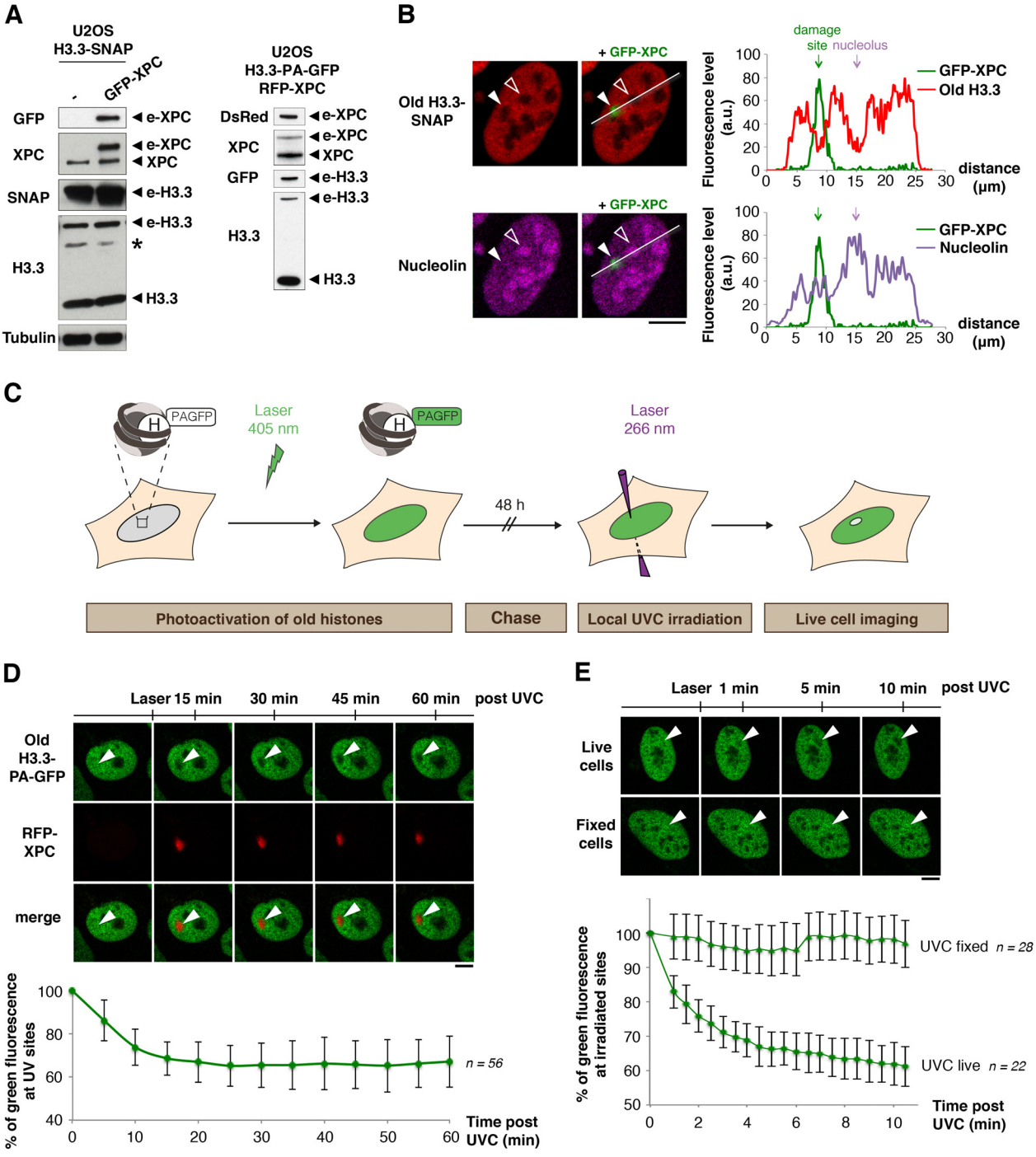
A
U2OS
H3.3-SNAP
-
GFP-XPC
GFP
XPC
SNAP
H3.3
Tubulin
◀ e-XPC
◀ e-XPC
◀ XPC
◀ e-H3.3
◀ e-H3.3
*
◀ H3.3
U2OS
H3.3-PA-GFP
RFP-XPC
DsRed
XPC
GFP
H3.3
◀ e-XPC
◀ e-XPC
◀ XPC
◀ e-H3.3
◀ e-H3.3
◀ H3.3
B
Old H3.3-SNAP
Nucleolin
+ GFP-XPC
+ GFP-XPC
damage site
nucleolus
GFP-XPC
Old H3.3
GFP-XPC
Nucleolin
Fluorescence level (a.u.)
distance (μm)
C
PAGFP
Laser 405 nm
48 h
Laser 266 nm
Photoactivation of old histones
Chase
Local UVC irradiation
Live cell imaging
D
Laser 15 min
30 min
45 min
60 min
post UVC
Old H3.3-PA-GFP
RFP-XPC
merge
% of green fluorescence at UV sites
n = 56
Time post UVC (min)
E
Laser 1 min
5 min
10 min
post UVC
Live cells
Fixed cells
% of green fluorescence at irradiated sites
UVC fixed n = 28
UVC live n = 22
Time post UVC (min)

Figure S1: Rapid decrease in parental H3 histone density in UVC-damaged chromatin regions. Related to Figure 1.

(A) Characterization by western blot of U2OS cell lines stably expressing H3.3-SNAP and GFP-XPC or H3.3-PA-GFP and RFP-XPC. e: epitope tag, *: aspecific band.

(B) Immunostaining for nucleolin in U2OS cells stably expressing H3.3-SNAP and GFP-XPC fixed 15 min after UVC laser micro-irradiation. Parental H3.3-SNAP histones were labeled in red as in Figure 1. Fluorescence profiles along the line crossing the UVC-damaged area (white arrowhead) and a nucleolus (empty arrowhead) are displayed on the graphs.

(C) Scheme of the experimental strategy for tracking parental histone dynamics at DNA damage sites based on photo-activation of PA-GFP-tagged H3.3 histones in the whole nucleus 48 h before UVC laser micro-irradiation and live cell imaging.

(D) Distribution of parental histones H3.3 (green) at the indicated time points after UVC laser micro-irradiation in U2OS cells stably expressing H3.3-PA-GFP and RFP-XPC.

(E) Dynamics of parental histones H3.3 (green) at early time points after local damage induced by UVC laser micro-irradiation as in (D). Paraformaldehyde-fixed cells were used as a control for photo-bleaching of the green fluorescence by the UVC laser. White arrowheads indicate the irradiated areas. The graphs show quantifications of the green fluorescence associated with parental H3.3 in irradiated areas, normalized to the green fluorescence in the same areas before laser micro-irradiation. Error bars represent SD from n cells scored in two independent experiments. Scale bars, 10 μm.

Figure S2

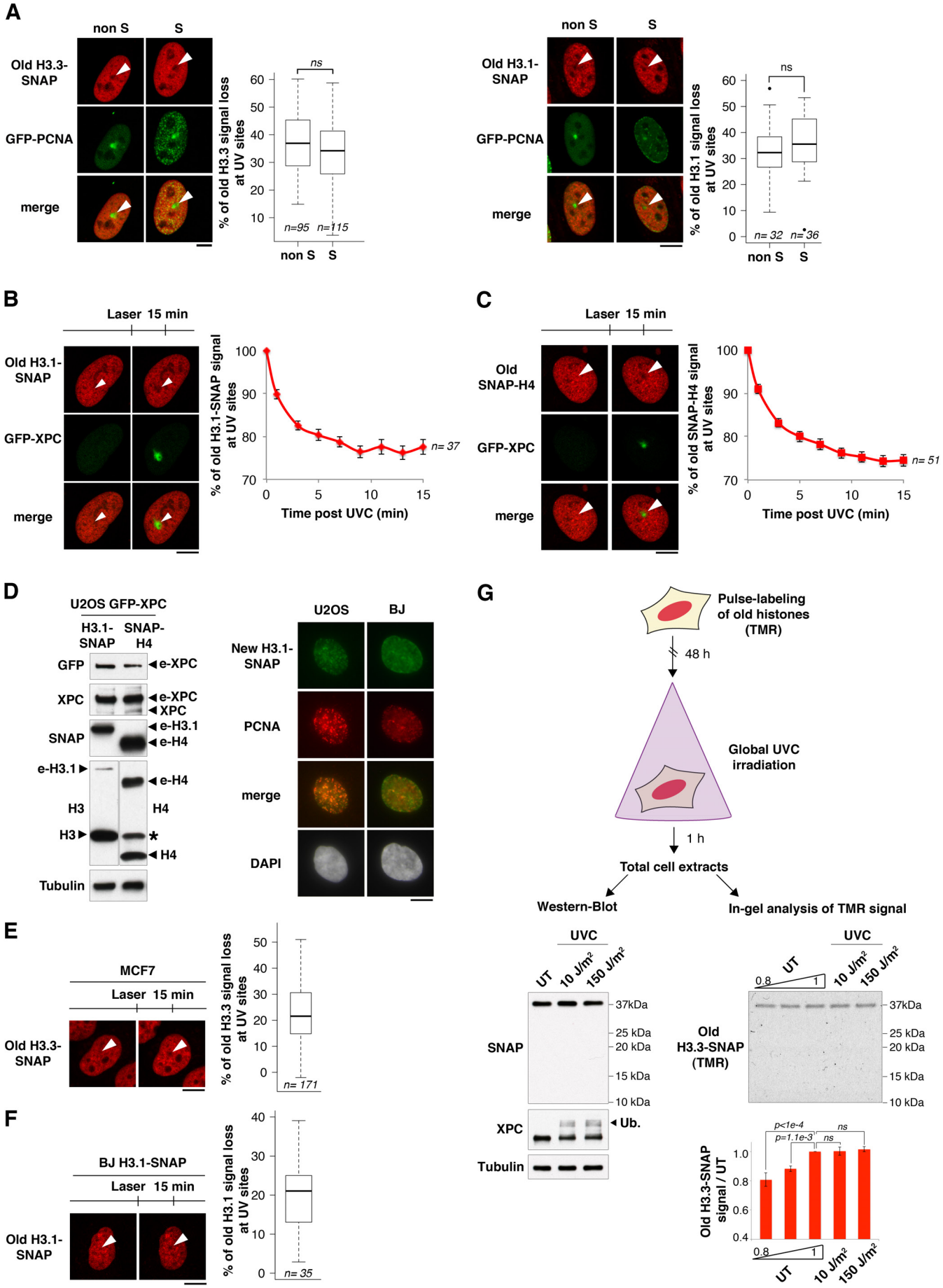
A
non S
S
Old H3.3-SNAP
GFP-PCNA
merge
% of old H3.3 signal loss at UV sites
ns
n=95 n=115
non S S
Old H3.1-SNAP
% of old H3.1 signal loss at UV sites
n= 32 n= 36
B
Laser 15 min
Old H3.1-SNAP
GFP-XPC
% of old H3.1-SNAP signal at UV sites
n= 37
Time post UVC (min)
C
Old SNAP-H4
% of old SNAP-H4 signal at UV sites
n= 51
D
U2OS GFP-XPC
H3.1-SNAP
SNAP-H4
GFP
XPC
SNAP
e-H3.1
H3
H4
Tubulin
e-XPC
e-H4
U2OS
BJ
New H3.1-SNAP
PCNA
merge
DAPI
E
MCF7
Laser 15 min
Old H3.3-SNAP
n= 171
F
BJ H3.1-SNAP
Old H3.1-SNAP
n= 35
G
Pulse-labeling of old histones (TMR)
48 h
Global UVC irradiation
1 h
Total cell extracts
Western-Blot
In-gel analysis of TMR signal
UVC
UT
10 J/m²
150 J/m²
SNAP
XPC
Ub.
Tubulin
37kDa
25 kDa
20 kDa
15 kDa
10 kDa
Old H3.3-SNAP (TMR)
Old H3.3-SNAP signal / UT
p<1e-4
p=1.1e-3
ns

Figure S2: Dynamics of parental H3 and H4 histones in UVC-damaged chromatin. Related to Figures 1 and 2.

(A) Distribution of parental histones H3.3 and H3.1 (red) 15 min after UVC laser micro-irradiation in U2OS cells stably expressing SNAP-tagged H3 variants and transiently transfected with GFP-PCNA. PCNA focal pattern is characteristic of S phase cells.

(B, C) Distribution of parental histones H3.1 (B) and H4 (C) before and 15 min after UVC laser micro-irradiation in U2OS cells stably expressing H3.1-SNAP or SNAP-H4 and GFP-XPC. White arrowheads indicate the irradiated areas. The graphs show quantifications of red fluorescence loss in irradiated areas as a function of time after laser micro-irradiation. Error bars represent SEM from n cells scored in two independent experiments.

(D) Characterization by western blot of U2OS lines stably expressing H3.1-SNAP or SNAP-H4 and GFP-XPC. e: epitope tag, *: aspecific band. We also verified by specific labeling of newly synthesized histones that new H3.1-SNAP displayed characteristic replication-coupled deposition patterns in U2OS and BJ cells. PCNA stains replication foci.

(E, F) Distribution of parental histones H3.3 (E) or H3.1 (F) before and 15 min after UVC laser micro-irradiation in MCF7 cells 96 h post H3.3-SNAP transfection (E) or in BJ cells stably expressing H3.1-SNAP (F). White arrowheads indicate the irradiated areas. The boxplots show quantifications of red fluorescence loss in irradiated areas at 15 min compared to before laser micro-irradiation (data from n cells scored in two independent experiments). Scale bars, 10 μm.

(G) Top: Scheme of the assay for analyzing old H3.3-SNAP protein levels. Global UVC irradiation was carried out at 10 J/m^2 (corresponding to the dose received by the whole nucleus upon laser micro-irradiation) or at 150 J/m^2 (corresponding to 25% of the dose received at the site of laser micro-irradiation for which we expect about 10% reduction in parental histone density at UV sites). Analysis of total H3.3-SNAP levels by western-blot (left) and measurement of old H3.3-SNAP levels by in-gel reading of TMR fluorescence (right) do not reveal any significant decrease in H3.3-SNAP protein levels nor any protein clipping upon UVC irradiation. Different amounts of untreated cell extracts (UT) were loaded to assess that a 10% signal reduction was detectable as shown on the graph quantifying TMR fluorescence intensity associated with H3.3-SNAP bands. XPC ubiquitylation (Ub.) is used as a control for UVC irradiation. ns: non significant.

Figure S3

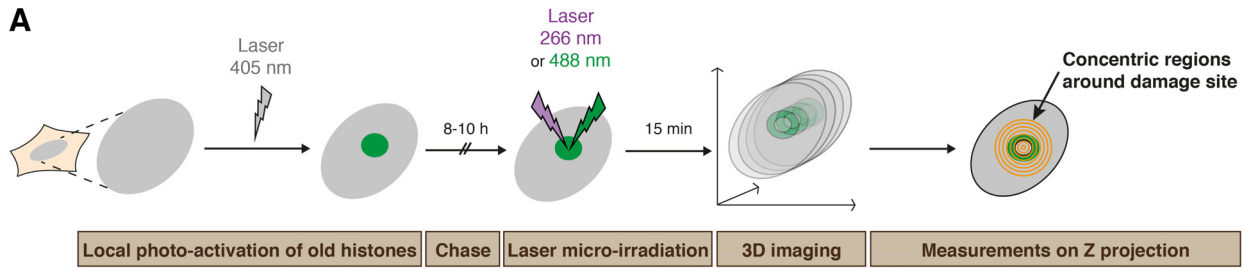
A
Laser
405 nm
Laser
266 nm
or 488 nm
8-10 h
15 min
Concentric regions
around damage site
Local photo-activation of old histones
Chase
Laser micro-irradiation
3D imaging
Measurements on Z projection

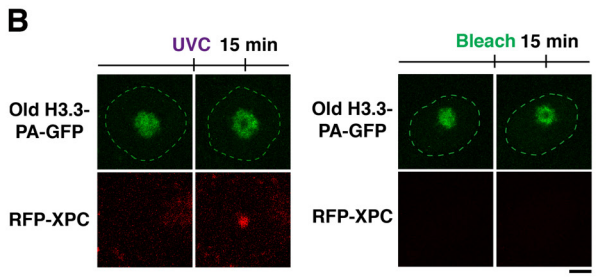
B
UVC 15 min
Bleach 15 min
Old H3.3-
PA-GFP
RFP-XPC

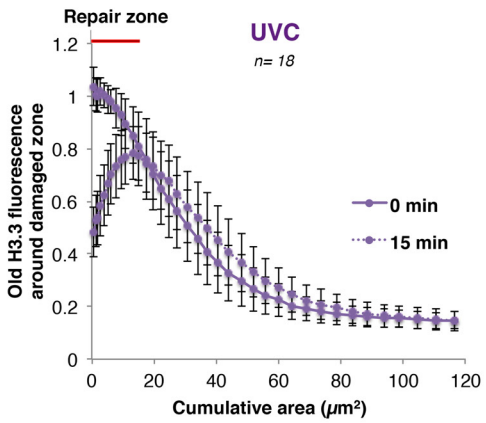
C
Repair zone
UVC
n= 18
Old H3.3 fluorescence
around damaged zone
0 min
15 min
Cumulative area (μm²)

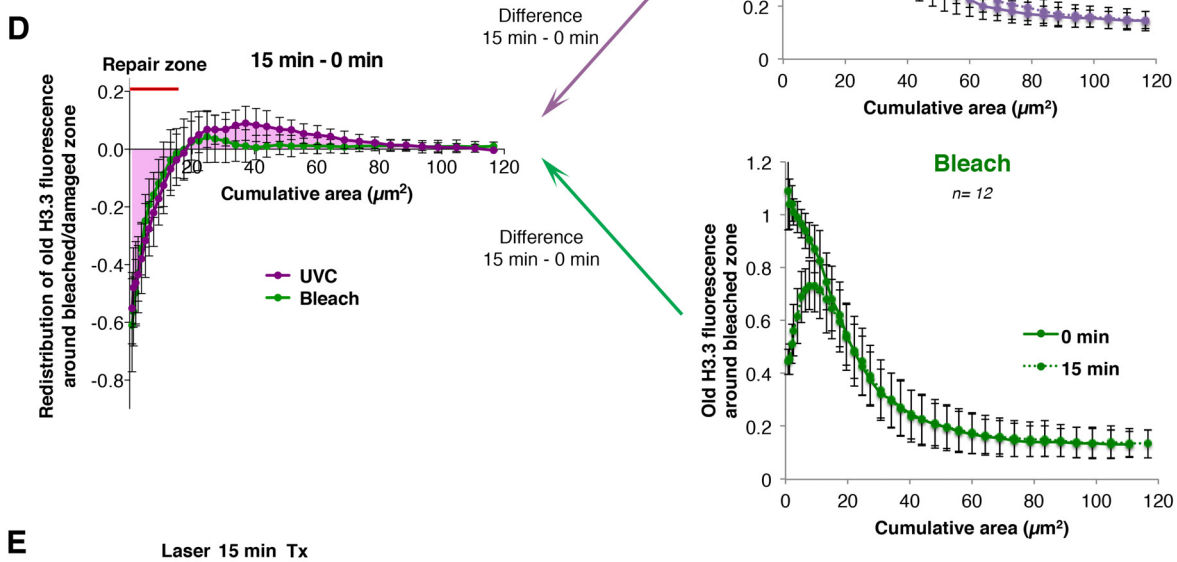
D
Repair zone
15 min - 0 min
Redistribution of old H3.3 fluorescence
around bleached/damaged zone
Cumulative area (μm²)
UVC
Bleach
Difference
15 min - 0 min
Difference
15 min - 0 min
Bleach
n= 12
Old H3.3 fluorescence
around bleached zone
0 min
15 min
Cumulative area (μm²)

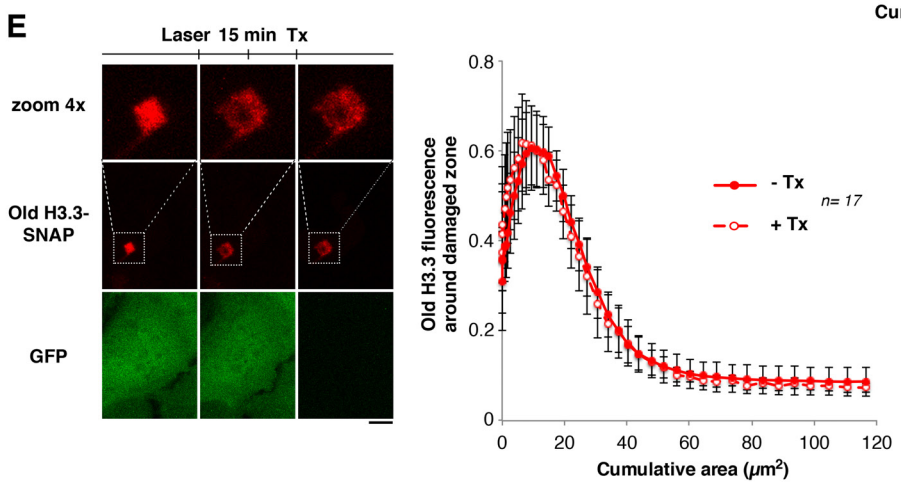
E
Laser 15 min Tx
zoom 4x
Old H3.3-
SNAP
GFP
Old H3.3 fluorescence
around damaged zone
- Tx
+ Tx
n= 17
Cumulative area (μm²)

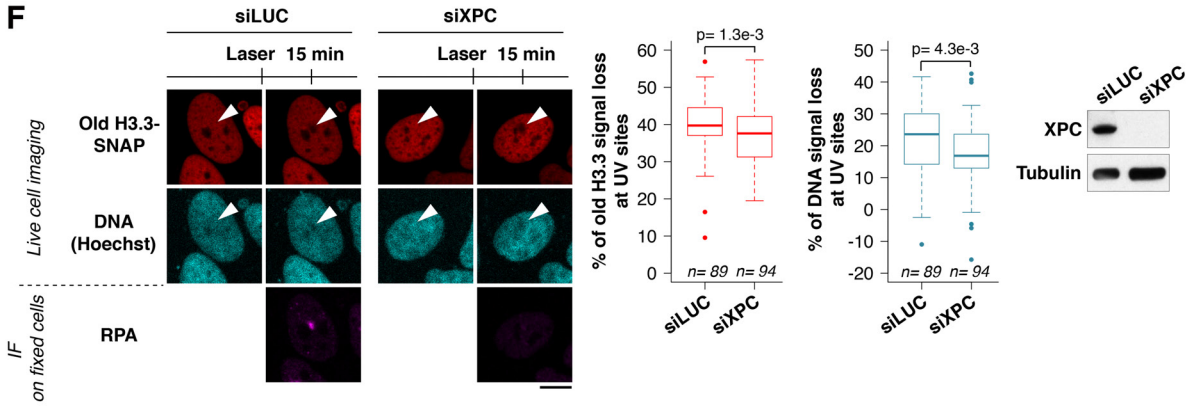
F
siLUC
siXPC
Laser 15 min
Laser 15 min
Live cell imaging
Old H3.3-
SNAP
DNA
(Hoechst)
IF
on fixed cells
RPA
% of old H3.3 signal loss
at UV sites
p= 1.3e-3
n= 89 n= 94
siLUC
siXPC
% of DNA signal loss
at UV sites
p= 4.3e-3
n= 89 n= 94
siLUC
siXPC
siLUC
siXPC
XPC
Tubulin

Figure S3: Conservative redistribution of parental histones to the periphery of UVC-damaged regions. Related to Figures 2 and 3.

(A) Experimental procedure for measuring parental histone loss and redistribution around the UVC damaged area based on photo-activation of a 20 μm^2 patch of pre-existing H3.3-PA-GFP histones in the cell nucleus and micro-irradiation in the center of the fluorescent histone patch with a 266 nm UVC laser (damage induction) or with a 488 nm bleaching laser (control). Fluorescence measurements are performed on 2D projections of 3D acquisitions in concentric regions around the site of laser micro-irradiation.

(B) Fluorescent patches of parental histones H3.3 (green) before and 15 min after local UVC damage (left) or local photo-bleaching (right) in U2OS cells stably expressing H3.3-PA-GFP and RFP-XPC. Green dotted lines delineate the cell nuclei.

(C) Quantification of the green fluorescence associated with parental H3.3-PA-GFP histones in concentric regions around the UVC damage site (purple) or the site of fluorescence bleaching with the 488 nm laser (green) at the indicated time points.

(**D**) Difference in green fluorescence distribution between the two time points obtained by subtracting 0 min from 15 min values quantified in (C). The positive and negative areas under the UVC curve (purple) are equivalent. The position of the repair zone is based on RFP-XPC accumulation at 15 min. Error bars represent SD from n cells scored in two independent experiments.

(E) Fluorescent patches of parental histones H3.3 (red) before and 15 min after UVC laser micro-irradiation, followed by detergent extraction (Tx) in live U2OS cells stably expressing H3.3-SNAP and GFP. GFP solubilization is used as a control for Tx extraction. The graph displays quantification of red fluorescence distribution in concentric regions around the UVC damage site before (-Tx) and after detergent extraction (+Tx). Error bars represent SD from n cells scored in two independent experiments.

(F) Distribution of parental histones H3.3 (red) and DNA (blue, stained with Hoechst) before and 15 min after local UVC irradiation in U2OS cells stably expressing H3.3-SNAP and treated with the indicated siRNAs (siLUC: control). XPC knock-down is verified by western-blot. Upon XPC downregulation, the exposure of single-stranded DNA that normally occurs during the repair process is impaired, as shown by the lack of RPA recruitment, but the reduction in Hoechst staining is still observed. The boxplot shows quantifications of histone (red) and DNA (blue) fluorescence loss in irradiated areas (data from n cells scored in two independent experiments). Scale bars, 10 μm.

Figure S4

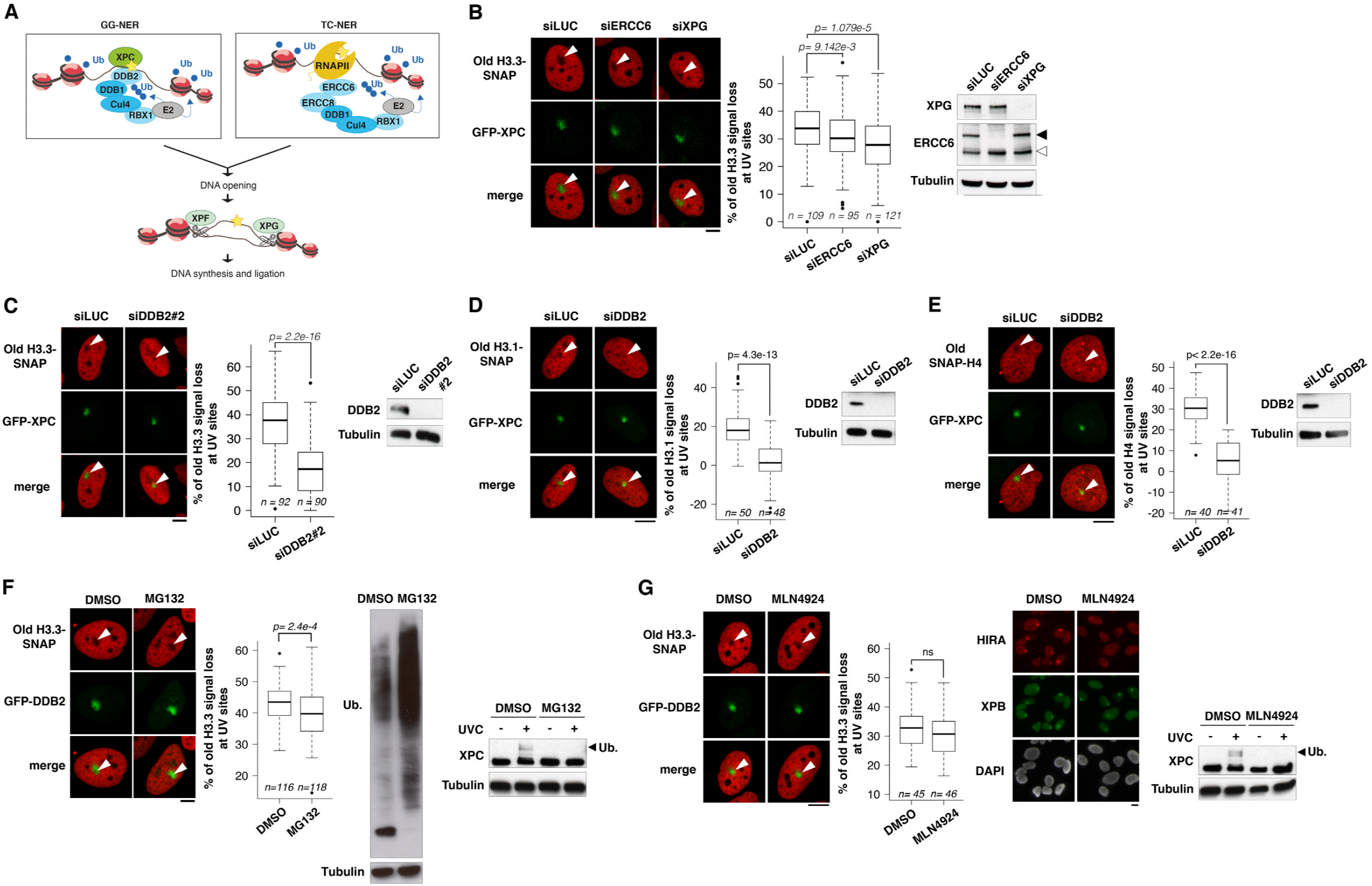
A
GG-NER
TC-NER
XPC
DDB2
DDB1
Cul4
RBX1
E2
Ub
RNAPII
ERCC6
ERCC8
DNA opening
XPF
XPG
DNA synthesis and ligation
B
siLUC
siERCC6
siXPG
Old H3.3-SNAP
GFP-XPC
merge
% of old H3.3 signal loss at UV sites
p= 1.079e-5
p= 9.142e-3
n = 109
n = 95
n = 121
XPG
ERCC6
Tubulin
C
siLUC
siDDB2#2
p= 2.2e-16
n = 92
n = 90
DDB2
D
siDDB2
Old H3.1-SNAP
% of old H3.1 signal loss at UV sites
p= 4.3e-13
n= 50
n= 48
E
Old SNAP-H4
% of old H4 signal loss at UV sites
p< 2.2e-16
n= 40
n= 41
F
DMSO
MG132
GFP-DDB2
% of old H3.3 signal loss at UV sites
p= 2.4e-4
n=116
n=118
Ub.
UVC
XPC
G
MLN4924
ns
n= 45
n= 46
HIRA
XPB
DAPI

Figure S4: Parental histone redistribution is controlled by the repair factor DDB2. Related to Figure 4.
(A) Simplified scheme of the NER pathway showing the different repair factors that were targeted by siRNAs in this study. GG-NER: Global Genome NER, TC-NER: Transcription-Coupled NER.
(B, C) Distribution of parental histones H3.3 (red) 15 min after UVC laser micro-irradiation in U2OS cells stably expressing H3.3-SNAP and GFP-XPC treated with the indicated siRNAs (siLUC: control). siRNA efficiencies were verified by western-blot. The black arrowhead indicates full-length ERCC6 and the empty arrowheads points to a splice variant.
(D, E) Distribution of parental histones H3.1 (D) and H4 (E) 15 min after UVC laser micro-irradiation in U2OS cells stably expressing H3.1-SNAP or SNAP-H4 and GFP-XPC treated with the indicated siRNAs (siLUC: control). siRNA efficiencies were verified by western-blot.
(F, G) Distribution of parental histones H3.3 (red) 15 min after UVC laser micro-irradiation in U2OS cells stably expressing H3.3-SNAP and GFP-DDB2 treated with the proteasome inhibitor MG132 (F) or the neddylation inhibitor MLN4924 (G) (DMSO, vehicle). The efficiency of MG132 treatment was verified by immunoblot against ubiquitin (Ub) showing the accumulation of non-degraded ubiquitylated proteins. Proteasome inhibition by MG132 thus affects *de novo* ubiquitylation by exhausting the pool of free ubiquitin as shown by the lack of XPC ubiquitylation post UVC irradiation. We controlled that the neddylation inhibitor also impairs UVC-induced ubiquitylation of XPC (western-blot) and HIRA accumulation at UVC damage sites (immunofluorescence) by interfering with the activity of the CUL4-DDB1-DDB2 complex. White arrowheads indicate the irradiated areas. Scale bars, 10 μm. The boxplots show quantifications of red fluorescence loss in irradiated areas at 15 min compared to before laser micro-irradiation (data from n cells scored in two independent experiments).

Figure S5

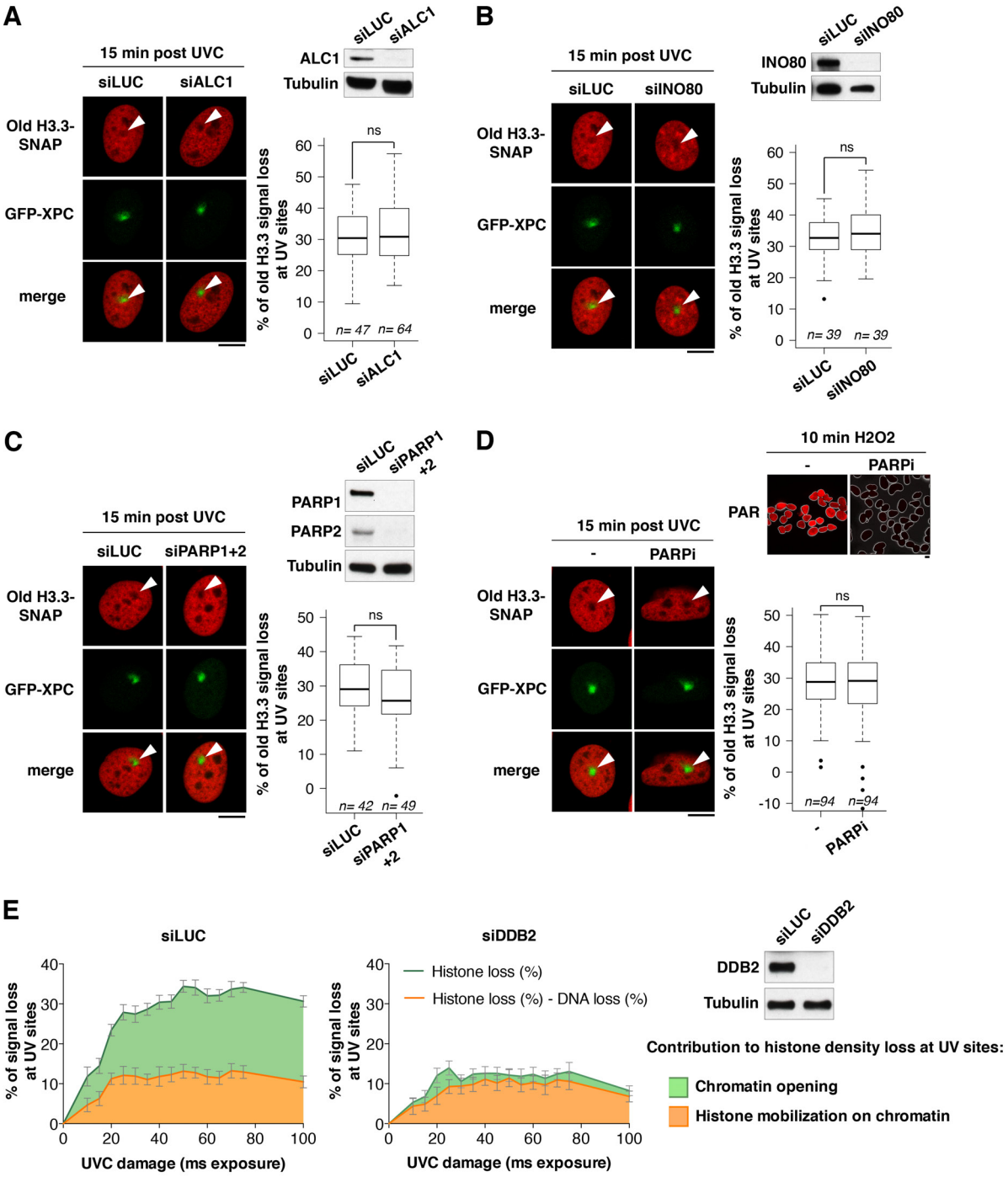
A
15 min post UVC
siLUC
siALC1
Old H3.3-SNAP
GFP-XPC
merge
ALC1
Tubulin
% of old H3.3 signal loss at UV sites
ns
n= 47
n= 64
B
siINO80
INO80
n= 39
n= 39
C
siPARP1+2
PARP1
PARP2
n= 42
n= 49
D
10 min H2O2
-
PARPi
PAR
n=94
n=94
E
siLUC
siDDB2
% of signal loss at UV sites
UVC damage (ms exposure)
Histone loss (%)
Histone loss (%) - DNA loss (%)
DDB2
Contribution to histone density loss at UV sites:
Chromatin opening
Histone mobilization on chromatin

Figure S5: Mechanistic insights into DDB2 function in parental histone dynamics. Related to Figures 3 and 4.

(A-C) Distribution of parental histones H3.3 (red) 15 min after UVC laser micro-irradiation in U2OS cells stably expressing H3.3-SNAP and GFP-XPC treated with the indicated siRNAs (siLUC: control). siRNA efficiencies were verified by western-blot.

(D) Distribution of parental histones H3.3 (red) 15 min after UVC laser micro-irradiation in U2OS cells stably expressing H3.3-SNAP and GFP-XPC treated or not with PARP inhibitor. The efficiency of PARP inhibition was verified by PAR staining after cell treatment with the oxidative agent H_2O_2. White lines delineate nuclear boundaries, based on DAPI staining. White arrowheads indicate the irradiated areas. Scale bars, 10 μm. The boxplots show quantifications of red fluorescence loss in irradiated areas at 15 min compared to before laser micro-irradiation (data from n cells scored in two independent experiments).

(E) Graphs showing chromatin opening (green) and histone mobilization on chromatin (orange) as a function of UVC damage in cells treated with the indicated siRNAs (siLUC: control). Results are based on measurements of parental H3.3 and DNA signal loss in irradiated areas as in Figure 3. DDB2 knock-down is verified by western-blot. Error bars represent SEM from at least 30 cells per time point scored in three independent experiments.

Figure S6

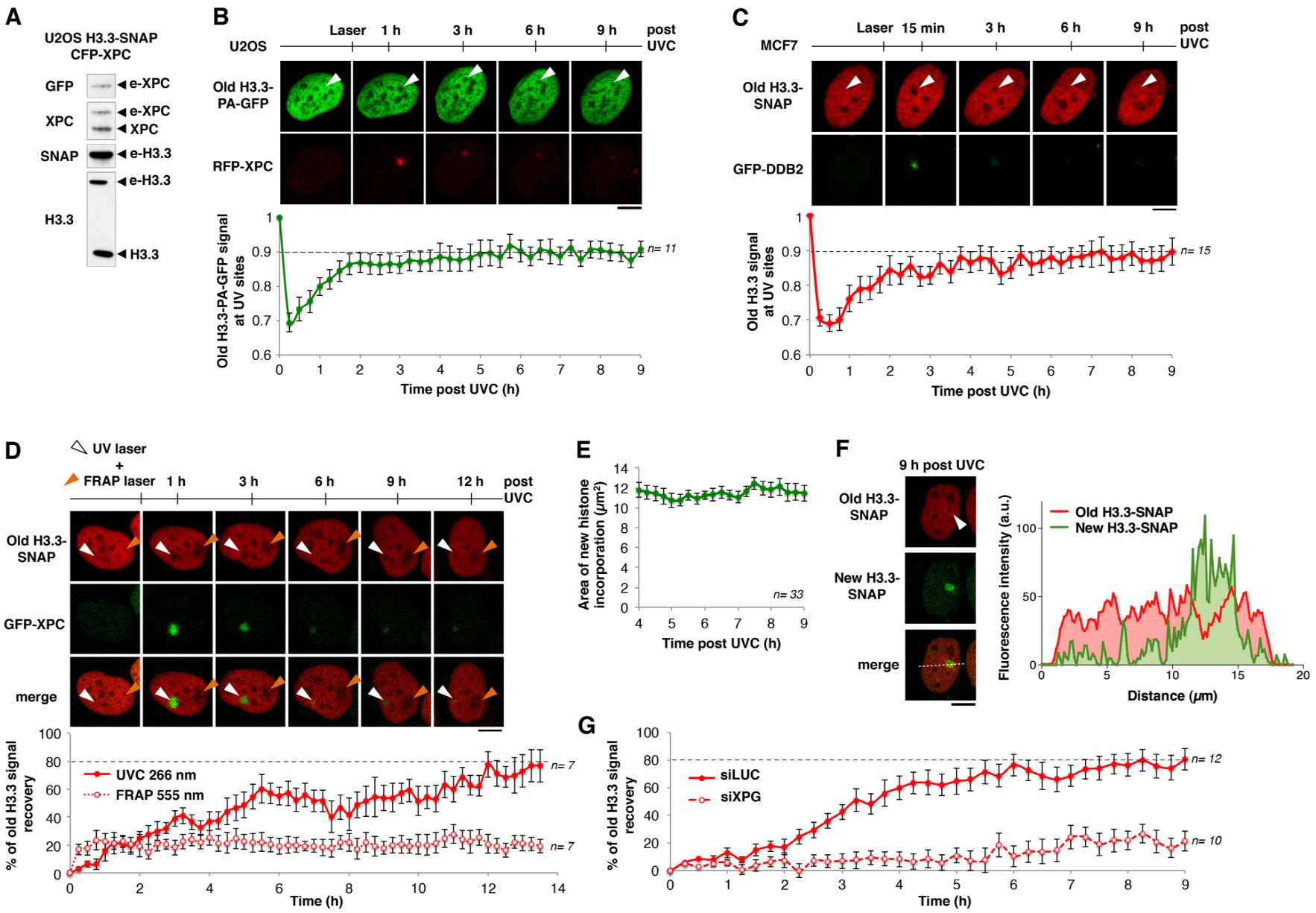
A
U2OS H3.3-SNAP CFP-XPC
GFP
XPC
SNAP
H3.3
e-XPC
e-XPC
XPC
e-H3.3
e-H3.3
H3.3
B
U2OS
Laser 1 h 3 h 6 h 9 h post UVC
Old H3.3-PA-GFP
RFP-XPC
Old H3.3-PA-GFP signal at UV sites
n= 11
Time post UVC (h)
C
MCF7
Laser 15 min 3 h 6 h 9 h post UVC
Old H3.3-SNAP
GFP-DDB2
Old H3.3 signal at UV sites
n= 15
Time post UVC (h)
D
UV laser
+
FRAP laser 1 h 3 h 6 h 9 h 12 h post UVC
Old H3.3-SNAP
GFP-XPC
merge
% of old H3.3 signal recovery
UVC 266 nm
FRAP 555 nm
n= 7
n= 7
Time (h)
E
Area of new histone incorporation (μm²)
n= 33
Time post UVC (h)
F
9 h post UVC
Old H3.3-SNAP
New H3.3-SNAP
merge
Old H3.3-SNAP
New H3.3-SNAP
Fluorescence intensity (a.u.)
Distance (μm)
G
% of old H3.3 signal recovery
siLUC
siXPG
n= 12
n= 10
Time (h)

Figure S6: Recovery of parental histones coupled to repair progression. Related to Figure 6.

(A) Characterization by western blot of the U2OS cell line stably expressing H3.3-SNAP and CFP-XPC. e: epitope tag.

(B) Dynamics of parental histones H3.3 (green) at the indicated time points after local UVC damage (white arrowheads) in U2OS cells stably expressing H3.3-PA-GFP and RFP-XPC. The graph shows quantification of green fluorescence in irradiated areas, normalized to before irradiation.

(C) Dynamics of parental histones H3.3 (red) at the indicated time points after local UVC damage (white arrowheads) in MCF7 cells transiently expressing H3.3-SNAP and GFP-DDB2. The graph shows quantification of red fluorescence in irradiated areas, normalized to before irradiation.

(D) Dynamics of parental histones H3.3 (red) at the indicated points after local damage with the UVC laser (white arrowheads) or after local bleaching of the red fluorescence with a 555 nm laser (orange arrowheads) in U2OS cells stably expressing H3.3-SNAP and GFP-XPC. The graph shows quantification of red fluorescence recovery in illuminated areas. Cells that did not repair efficiently (based on GFP-XPC retention) were excluded from the analysis.

(E) Graph showing the area occupied by newly incorporated H3.3 at the indicated time points after local damage in U2OS cells stably expressing H3.3-SNAP and CFP-XPC. The analysis starts at 4 h post UVC, when new histone deposition reaches a plateau (Figure 6A).

(F) Distribution of parental (red) and newly synthesized H3.3 (green) 9 h after local UVC damage (white arrowhead). Fluorescence profiles along the dotted line crossing the UVC-damaged area are displayed on the graph. a.u.: arbitrary units.

(G) Graph showing the quantification of red fluorescence recovery in irradiated areas in U2OS cells stably expressing H3.3-SNAP and GFP-DDB2 and treated with the indicated siRNAs (data from Figure 5B).

Fluorescence recovery at time t (D and G panels) is calculated as (It-Imin)/(I0-Imin) where 'I' represents the red fluorescence intensity in the illuminated area relative to the entire nucleus, 'I0' is the intensity before irradiation and 'Imin' is the lowest intensity measured. Error bars on the graphs represent SEM from n cells scored in two independent experiments. Scale bars, 10 μm.

SUPPLEMENTAL MOVIES

Movie S1: Parental H3.3 dynamics after local UVC damage (10 min kinetics). Related to Figure 1C.
Dynamics of parental histones H3.3 (red) during the first 10 min after local damage with the UVC laser in U2OS cells stably expressing H3.3-SNAP. 21 images were captured at 30 sec intervals and are displayed at 2 frames/sec. The resulting motion picture is shown with a superimposed white arrowhead pointing to the laser irradiation site.

Movie S2: New H3.3 dynamics after local UVC damage (2 h kinetics). Related to Figure 5A.
Dynamics of newly synthesized histones H3.3 (green) during the first 2 h after local damage with the UVC laser in U2OS cells stably expressing H3.3-SNAP. 25 images were captured at 5 min intervals and are displayed at 2 frames/sec. The resulting motion picture is shown with a superimposed white arrowhead pointing to the laser irradiation site.

Movie S3: Parental H3.3 dynamics after local UVC damage (2 h kinetics). Related to Figure 5A.
Dynamics of parental histones H3.3 (red) during the first 2 h after local damage with the UVC laser in U2OS cells stably expressing H3.3-SNAP. 25 images were captured at 5 min intervals and are displayed at 2 frames/sec. The resulting motion picture is shown with a superimposed white arrowhead pointing to the laser irradiation site.

Movie S4: Parental H3.3 dynamics after local UVC damage (12 h kinetics). Related to Figure 6C.
Dynamics of parental histones H3.3 (red) during the first 12 h after local damage with the UVC laser in U2OS cells stably expressing H3.3-SNAP and GFP-DDB2 treated with siRNA control siLUC. 49 images were captured at 15 min intervals and are displayed at 4 frames/sec. The resulting motion picture (red channel only) is shown with a superimposed white arrowhead pointing to the laser irradiation site.

Movie S5: Parental H3.3 dynamics after local UVC damage (12 h kinetics) in repair-deficient cells. Related to Figure 6C.
Dynamics of parental histones H3.3 (red) during the first 12 h after local damage with the UVC laser in U2OS cells stably expressing H3.3-SNAP and GFP-DDB2 treated with siXPG. 49 images were captured at 15 min intervals and are displayed at 4 frames/sec. The resulting motion picture (red channel only) is shown with a superimposed white arrowhead pointing to the laser irradiation site.

SUPPLEMENTAL EXPERIMENTAL PROCEDURES

Stable cell lines

For stable cell line establishment, U2OS cells were transfected with plasmid DNA 48 h before antibiotic selection of clones. The BJ polyclonal cell line expressing H3.1-SNAP-3xHA was obtained by retroviral transduction. All cell lines were grown at 37°C and 5% CO_2 in Dulbecco's modified Eagle's medium (DMEM, Invitrogen) supplemented with 10% fetal calf serum (EUROBIO), 100 U/mL penicillin and 100 µg/mL streptomycin (Invitrogen) and the appropriate selection antibiotics: Blasticidin (5 µg/ml, Invitrogen), G418 (100 µg/mL, Invitrogen), Hygromycin (200 µg/mL, Euromedex).

Cell line (reference)	Selection antibiotics
BJ H3.1-SNAP-3xHA	Blasticidin
MCF7	None
U2OS H3.3-SNAP (Dunleavy et al., 2011)	G418
U2OS H3.3-SNAP GFP	G418
U2OS H3.3-SNAP GFP-XPC	G418 + Hygromycin
U2OS H3.3-SNAP CFP-XPC	G418 + Hygromycin
U2OS H3.3-SNAP GFP-DDB2	G418 + Hygromycin
U2OS H3.1-SNAP GFP-XPC (U2OS H3.1 SNAP from Dunleavy et al., 2011)	G418 + Hygromycin
U2OS SNAP-H4 GFP-XPC	G418 + Hygromycin
U2OS H3.3-PA-GFP RFP-XPC	G418 + Hygromycin
U2OS LacO H3.3-SNAP (U2OS LacO with 256 tandem LacO repeats from Beuzer et al., 2014; Soutoglou et al., 2007)	G418

Plasmids.

All the coding sequences for histone variants and repair factors are of human origin except lacR-fused DDB2, which is murine. All constructs were verified by direct sequencing and/or restriction digests. Cloning details and primer sequences (Sigma-Aldrich) are available upon request.

Plasmid	Construct details
H3.3-SNAP	*H3F3B* coding sequence cloned into pSNAPm (New England Biolabs) (Dunleavy et al., 2011)
H3.1-SNAP	*HIST1H3C* coding sequence cloned into pSNAPm (New England Biolabs) (Dunleavy et al., 2011)
H3.1-SNAP-3xHA	pBABE-Blasti H3.1-SNAP-3xHA plasmid described in (Ray-Gallet et al., 2011)
H3.3-PA-GFP	*H3F3B* coding sequence in frame with PA-GFP in PA-GFP-N1 (Patterson and Lippincott-Schwartz, 2004) subcloned into pSNAPm replacing the SNAP tag sequence
SNAP-H4	*HIST1H4J* coding sequence cloned into pSNAPm (New England Biolabs)
GFP	pEGFP-C1 (Clontech)
GFP-PCNA	(Leonhardt et al., 2000)
GFP-XPC	Flag-GFP-XPC in pIREShyg (Clontech) (Nishi et al., 2009)
RFP-XPC	RFP from mRFP-C1 (Campbell et al., 2002) subcloned into CFP-XPC plasmid, replacing CFP
CFP-XPC	CFP-XPC (Montpellier Genomic Collections) subcloned into pBabe Hygro (Cell Biolabs)
GFP-DDB2	*DDB2* coding sequence (Montpellier Genomic Collections) subcloned into GFP-XPC plasmid, replacing XPC
mCherry-lacR	mCherry-lacR-NLS (Soutoglou and Misteli, 2008)
mCherry-lacR-DDB2	DDB2 in mCherry-lacR (Luijsterburg et al., 2012)

Drug treatments

DNA was stained by incubating live cells with Hoechst 33258 (10 µg/mL final concentration, Sigma-Aldrich) for 30 min at 37°C before the analysis. Detergent extraction on live cells was performed with 0.5% Triton-X-100 in CSK buffer (Cytoskeletal buffer: 10 mM PIPES pH 7.0, 100 mM NaCl, 300 mM sucrose, 3 mM $MgCl_2$). The PARP inhibitor KU-58948 (gift from S. Jackson laboratory) was added to the culture medium at 10 µM final

concentration 1 h before irradiation. The neddylation inhibitor MLN4924 (Merck Millipore) was added to the culture medium at 2 μM final concentration 30 min before irradiation. Proteasome inhibition was performed by adding MG132 to the culture medium for 2 h at 37°C before the analysis (10 μM final concentration, Enzo Life Science). Treatment of cells with H_2O_2 (1 mM final, VWR Chemicals) was for 10 min on ice. LacR-DDB2 release from the Lac operator was achieved by adding IPTG (isopropyl β-D-1-thiogalactopyranoside, 10 mM final concentration, Euromedex) to the culture medium in which the usual serum is replaced by Tetracycline-free fetal calf serum (Biowest). For long-term experiments on live cells, Hepes buffer was added to the culture medium (25 mM final concentration, Sigma-Aldrich).

siRNA sequences.
All siRNAs were purchased from Eurofins MWG Operon. The final concentration of each siRNA in the culture medium was 50 nM. Cells were analyzed and/or harvested 72 h post-transfection. When performing over-night experiments with mixed cell populations treated with different siRNAs, one of the two cell populations was stained with Cell Tracker Deep Red (Life Technologies) following manufacturer's instructions.

Designation	Target sequence
siALC1	5' UCUACUCCCUCCUCAGUUU 3'
siCUL4A	5'GAAUCCUACUGCUGAUCGA3'
siDDB1	5'GCAAGGACCUGCUGUUUAU3'
siDDB2	5'UCACUGGGCUGAAGUUUAA3',
siDDB2#2	5'UCAGUUCGCUUAAUGAAUU3'
siERCC6	5'GAAGAGUUGUCAGUGAUUA3'
siH3.3	1:1 combination of siH3.3A: 5'CUACAAAAGCCGCUCGCAA3' and siH3.3B: 5'GCUAAGAGAGUCACCAUCAU3'
siHIRA	5'GGAGAUGACAAACUGAUUA3'
siINO80	5' GGAGUUAUUUGAACGGCAA 3'
siLUC (Luciferase)	5'CGUACGCGGAAUACUUCGA3'
siPARP1	5' GGGCAAGCACAGUGUCAAA 3'
siPARP2	5' AGAUGAUGCCCAGAGGAAC 3'
siXPC	5' GCAAAUGGCUUCUAUCGAA 3'
siXPG	5'GAAAGAAGAUGCUAAACGU3'

SNAP labeling and photo-activation of histones
Pre-existing SNAP-tagged histones were labeled by incubating cells with 2 μM red-fluorescent SNAP reagent (SNAP-cell TMR star, New England Biolabs) or 4 μM green-fluorescent SNAP reagent (SNAP-cell Oregon Green, New England Biolabs) for 20 min (pulse), followed by a 30 min-incubation in fresh medium. Cells were subject to laser micro-irradiation and imaging 48 h after the pulse.
For specific labeling of newly-synthesized histones, pre-existing SNAP-tagged histones were first quenched by incubating cells with 10 μM SNAP-cell Block (New England Biolabs) for 30 min followed by a 30 min-wash in fresh medium and a 2 h-chase. The SNAP-tagged histones neo-synthesized during the chase were then pulse-labeled as described above. Cells were subject to local UVC irradiation immediately afterwards.
Laser settings for photo-activation were: maximum power, 5 iterations, 6.30 μsec/pixel scan speed. We photo-activated either total nuclei 48 h prior to local UVC irradiation or a nuclear region of 50 μm^2 8 to 10 h before local UVC irradiation to minimize the distortion of the photo-activated area due to cell movement and cell division.

UVC laser micro-irradiation
For laser-induction of UVC damage, cells were grown on quartz coverslips (SPI supplies) and irradiated for 50 ms unless stated otherwise using a 2 mW pulsed diode-pumped solid-state laser emitting at 266 nm (repetition rate up to 10 kHz, Rapp OptoElectronics, Hamburg GmbH) on a Zeiss LSM 700 confocal microscope adapted for UVC transmission with all-quartz optics. The laser was attenuated using a neutral density filter OD1 (10%T) and focused through a quartz 40x/0.6 Ultrafluar glycerol objective (Carl Zeiss) to yield a spot size of 2 μm in diameter, damaging ca. 2% of the nuclear volume. In these conditions, UVC laser damage did not cause major cytotoxicity as the mortality rate over a 14 h live cell imaging experiment after laser damage was only around 10% and damaged cells did repair and went through mitosis. The UVC dose delivered at the site of laser micro-irradiation was estimated at 600 J/m^2 - corresponding to ca. 1 UV lesion per nucleosome - by comparing the intensity of GFP-XPC recruitment upon local UVC irradiation in the same nucleus with the 266 nm laser and with a 254 nm lamp through a micropore filter (Millipore). The dose delivered by the UVC lamp was measured with a VLX-3W dosimeter (Vilbert-Lourmat).

Local UVC irradiation through micropore filters
Cells grown on glass coverslips (VWR) were covered with a polycarbonate filter (5 μm pore size, Millipore) and irradiated with 150 J/m^2 UVC (254 nm) using a low-pressure mercury lamp. Conditions were set using a VLX-3W dosimeter (Vilbert-Lourmat).

FRAP (Fluorescence Recovery After Photo-bleaching)
Bleaching of the red fluorescence was performed on a Zeiss LSM700 confocal microscope with a 10 mW 555 nm laser (laser settings: maximum power, 4 iterations, 1.58 μ sec/pixel scan speed). Bleaching of the green fluorescence was performed using a 10 mW 488 nm laser (laser settings: maximum power, 15 iterations, 6.30 μ sec/pixel scan speed). In both cases, the laser was focused through a LD LCI Plan-Apochromat 25x/0.8 multi-immersion objective, the bleached area was 10 μm^2 and bleaching conditions were set to reach a local loss of fluorescence similar to the loss of signal observed 15 min after UVC laser damage. For bleaching of the red fluorescence in the entire nucleus to leave a small fluorescent patch of 20-25 μm^2, the laser settings were changed to 10 iterations and 12.61 μ sec/pixel scan speed.

Image acquisition and analysis
Live cell imaging of LacR-DDB2 dynamics was performed on a Zeiss LSM710 confocal microscope using a Plan-Apochromat 63x/1.4 oil objective. Live cell imaging coupled to local UVC irradiation was performed using a LD LCI Plan-Apochromat 25x/0.8 multi-immersion objective on a Zeiss LSM700 confocal microscope equipped with a UVC laser to inflict damage and adapted for UVC transmission with all quartz optics. Cells were kept at 37°C during acquisition using a microscope incubator system (PeCon). The fluorescence-based autofocus mode was activated in order to acquire images from the best focal plane. Image J software (U. S. National Institutes of Health, Bethesda, Maryland, USA, http://imagej.nih.gov/ij/) was used for image analysis. To correct for overall bleaching of the signal due to repetitive imaging, fluorescence intensities were normalized against intensities measured in an undamaged nucleus in the same field. The extent of fluorescence loss at irradiated sites was determined by dividing the fluorescence intensity in the illuminated area by the fluorescence intensity of the entire nucleus, after background subtraction. The illuminated area was defined at 10-15 min post irradiation, based on fluorescently-labeled XPC or based on fluorescence loss, and was kept the same for all time points. Fluorescence recovery in the illuminated region was calculated relative to before illumination and starting from the time point with minimum intensity. The areas of low parental histone density and of new histone incorporation were measured using the inbuilt Moments threshold (on inverted images for parental histone signal). The GFP-XPC and CPD areas (damaged chromatin) were measured using the inbuilt Yen threshold (set from 20 to 225 for CPD measurement). In this analysis, we verified that there was no significant difference in CPD signals (Integrated Density) between 0 and 15 min post UVC, which is expected given the long time scale of CPD repair. 2D projections of 3D images from z-stack acquisitions (Figure 2 and S2) were obtained by maximum intensity z-projection (note that comparable results were obtained when running image analyses on 3D acquisitions and on maximum intensity projections using Imaris software). On these projections, fluorescence intensity was measured in the micro-irradiated zone, in the entire nucleus and in concentric circular regions spaced by 1 pixel and centered on the laser micro-irradiation site using a custom Image J macro. In this analysis, we systematically verified that the largest circle was within the boundaries of the cell nucleus.

Cell extracts and western blot
Total extracts were obtained by scraping cells in Laemmli buffer (50 mM Tris HCl pH 6.8, 1.6% SDS (Sodium Dodecyl Sulfate), 8% glycerol, 4% β-mercaptoethanol, 0.0025% bromophenol blue) followed by 5 min denaturation at 95°C. For western blot analysis, extracts were run on 4%–20% Mini-PROTEAN TGX gels (Bio-Rad) in running buffer (200 mM glycine, 25 mM Tris, 0.1% SDS) and transferred onto nitrocellulose membranes (Protran) with a Trans-Blot SD semidry transfer cell (Bio-Rad). Total proteins were revealed by reversible protein stain (Pierce). Proteins of interest were probed using the appropriate primary and HRP (Horse Radish Peroxidase)-conjugated secondary antibodies (Jackson Immunoresearch), detected using Super-Signal West Pico or Femto chemiluminescence substrates (Pierce).

Immunofluorescence
Cells grown on glass coverslips (VWR) were fixed directly with 2% paraformaldehyde and permeabilized with 0.2% Triton X-100 in PBS or pre-extracted before fixation with 0.5% Triton-X-100 in CSK buffer (Cytoskeletal buffer: 10 mM PIPES pH 7.0, 100 mM NaCl, 300 mM sucrose, 3 mM $MgCl_2$) for 5 min. Methanol fixation was used for PCNA staining. For CPD staining, DNA was denatured with 0.5 M NaOH for 5 min. Samples were blocked in 5% BSA (Bovine Serum Albumin, Sigma-Aldrich) in PBS supplemented with 0.1% Tween before incubation with primary antibodies and secondary antibodies conjugated to Alexa-Fluor dyes (Invitrogen). Coverslips were mounted in Vectashield medium with DAPI (Vector laboratories).

Antibodies

	Antibody	Species	Dilution	Application	Supplier (reference)
Primary	**ALC1**	Mouse	1:1000	WB	Abcam (ab51324)
	CPD	Mouse	1:1000	IF	Kamiya Biomedical Company (MC-062)
	CUL4A	Rabbit	1:2000	WB	Bethyl Laboratories (A300-739A)
	DDB1	Rabbit	1:2000	WB	Abcam (ab21080)
	DDB2	Mouse	1:200	WB	Abcam (ab51017)
	DsRed	Rabbit	1:1000	WB	Clontech (632496)
	ERCC6	Rabbit	1:500	WB	Santa Cruz Biotechnology (sc-25370)
	GFP	Mouse	1:1000	WB	Roche Applied Science (11814460001)
	H3	Rabbit	1:500	WB	Sigma Aldrich (H9289)
	H3.3	Mouse	1:200	WB	Abnova (H00003021-M01)
	H4	Rabbit	1:1000	WB	Cell Signaling Technology (13919)
	HIRA	Mouse	1:200/1:100	WB/IF	Active Motif (39557)
	INO80	Rabbit	1:1000	WB	Euromedex (A303-371A)
	Nucleolin	Rabbit	1:1000	IF	Santa Cruz Biotechnology (sc-13057)
	PAR	Rabbit	1:100	IF	Trevigen (4336-BPC-100)
	PARP1	Rabbit	1:1000	WB	Cell Signaling Technology (9542)
	PARP2	Rabbit	1:1000	WB	Enzo Life Sciences (ALX-210-303)
	PCNA	Mouse	1:1000	IF	DAKO (M0879)
	RPA	Mouse	1:500	IF	Abcam (ab2175)
	SNAP	Rabbit	1:1000	WB	Pierce Antibodies (CAB4255)
	Tubulin	Mouse	1:10 000	WB	Sigma-Aldrich (T9026)
	XPB	Rabbit	1:400	IF	Santa Cruz Biotechnology (sc-293)
	XPC	Mouse	1:500	WB	Genetex (GTX70294)
	XPG	Rabbit	1:500	WB	Bethyl Laboratories (A301-484A)
Secondary	**Anti-Mouse HRP**	Goat	1:10 000	WB	Jackson Immunoresearch (115-035-068)
	Anti-Rabbit HRP	Donkey	1:10 000	WB	Jackson Immunoresearch (711-035-152)
	Anti-Rabbit Alexa Fluor 680	Goat	1:1000	IF	Invitrogen (A21109)
	Anti-Mouse Alexa Fluor 647	Goat	1:1000	IF	Invitrogen (A21236)
	Anti-Mouse Alexa Fluor 594	Goat	1:1000	IF	Invitrogen (A11032)
	Anti-Rabbit Alexa Fluor 594	Goat	1:1000	IF	Invitrogen (A11037)
	Anti-Rabbit Alexa Fluor 488	Goat	1:1000	IF	Invitrogen (A11034)

Quantification of parental histone protein amounts following global UVC irradiation

Parental H3.3-SNAP histones were labeled by incubating U2OS H3.3-SNAP cells with 2 µM SNAP-cell TMR star (New England Biolabs) for 20 min. Cells were globally irradiated 48 h later with UVC (254 nm) at the indicated doses using a low-pressure mercury lamp. Conditions were set using a VLX-3W dosimeter (Vilbert-Lourmat). One hour after irradiation, cells were harvested in Laemmli buffer. Total protein concentration in each sample was measured on a DS-11 FX+ spectrophotometer (DeNovix). Equal protein amounts were loaded on 4%–20% Mini-PROTEAN TGX gels (Bio-Rad) for electrophoresis followed by western-blot or in-gel

fluorescence analysis of TMR-star fluorescence with a Typhoon FLA-7000 (GE Healthcare-Life Sciences). The intensities of fluorescent bands corresponding to TMR star-labeled parental H3.3-SNAP were quantified using ImageJ software.

Quantitative RT-PCR

RNA extracted from cells with Trizol (Invitrogen) and precipitated in isopropanol was subject to DNA digestion with Turbo DNA-free (Life technologies) and reverse transcribed with Superscript III RT using random primers (Life technologies). Quantitative PCR reactions were carried out with the indicated primer pairs and the Power SYBR® Green PCR Master Mix (Life Technologies) and read in 96-well plates (MicroAmp® Fast Optical, Life Technologies) using a ABI 7500 Fast detection system (Life Technologies). Results were normalized to the amount of the GAPDH gene product.

PCR primers

Designation	Sequence	Final concentration	Supplier
H3F3A_F	$^{5'}$GATGGCAACTAAATGGTGTTTG$^{3'}$	500 nM	Eurofins MWG Operon
H3F3A_R	$^{5'}$CAGGAACAGCACAGAAGACAG$^{3'}$		
H3F3B_F	$^{5'}$CAACCCAGAAGGCGAAGATA$^{3'}$		
H3F3B_R	$^{5'}$TTTCTCCTTTGCCTCTGCTC$^{3'}$		
GAPDH_F	$^{5'}$CAAGGCTGTGGGCAAGGT$^{3'}$		
GAPDH_R	$^{5'}$GGAAGGCCATGCCAGTGA$^{3'}$		

F : forward ; R : reverse.

SUPPLEMENTAL REFERENCES

Beuzer, P., Quivy, J.-P., and Almouzni, G. (2014). Establishment of a replication fork barrier following induction of DNA binding in mammalian cells. Cell Cycle *13*, 1607–1616.

Campbell, R.E., Tour, O., Palmer, A.E., Steinbach, P.A., Baird, G.S., Zacharias, D.A., and Tsien, R.Y. (2002). A monomeric red fluorescent protein. Proc. Natl. Acad. Sci. U.S.a. *99*, 7877–7882.

Dunleavy, E.M., Almouzni, G., and Karpen, G.H. (2011). H3.3 is deposited at centromeres in S phase as a placeholder for newly assembled CENP-A in G1 phase. Nucleus *2*, 146–157.

Leonhardt, H., Rahn, H.P., Weinzierl, P., Sporbert, A., Cremer, T., Zink, D., and Cardoso, M.C. (2000). Dynamics of DNA replication factories in living cells. J. Cell Biol. *149*, 271–280.

Luijsterburg, M.S., Lindh, M., Acs, K., Vrouwe, M.G., Pines, A., van Attikum, H., Mullenders, L.H., and Dantuma, N.P. (2012). DDB2 promotes chromatin decondensation at UV-induced DNA damage. J. Cell Biol. *197*, 267–281.

Nishi, R., Alekseev, S., Dinant, C., Hoogstraten, D., Houtsmuller, A.B., Hoeijmakers, J.H.J., Vermeulen, W., Hanaoka, F., and Sugasawa, K. (2009). UV-DDB-dependent regulation of nucleotide excision repair kinetics in living cells. DNA Repair (Amst.) *8*, 767–776.

Patterson, G.H., and Lippincott-Schwartz, J. (2004). Selective photolabeling of proteins using photoactivatable GFP. Methods (San Diego, Calif) *32*, 445–450.

Ray-Gallet, D., Woolfe, A., Vassias, I., Pellentz, C., Lacoste, N., Puri, A., Schultz, D.C., Pchelintsev, N.A., Adams, P.D., Jansen, L.E.T., et al. (2011). Dynamics of histone H3 deposition in vivo reveal a nucleosome gap-filling mechanism for H3.3 to maintain chromatin integrity. Mol. Cell *44*, 928–941.

Soutoglou, E., and Misteli, T. (2008). Activation of the cellular DNA damage response in the absence of DNA lesions. Science *320*, 1507–1510.

Soutoglou, E., Dorn, J.F., Sengupta, K., Jasin, M., Nussenzweig, A., Ried, T., Danuser, G., and Misteli, T. (2007). Positional stability of single double-strand breaks in mammalian cells. Nat. Cell Biol. *9*, 675–682.